

ulm university universität  
**ulm**

MASTER THESIS

---

**Simulation and modeling of grain growth  
using a misorientation-dependent phase  
field model**

---

*Author:*

Anton Manin

*Supervisor:*

M.Sc. Mingyan Wang

*Examiners:* Prof. Carl E. Krill, Ph.D.  
Prof. Dr. Peter Unger

October 2015



## **Declaration of Authorship**

I, Anton Manin, declare that this presented thesis is my own work. I confirm that I have acknowledged all main sources of help.

Signed:

Date:



# Contents

<b>Declaration of Authorship</b>	<b>iii</b>
<b>Contents</b>	<b>v</b>
<b>1 Introduction</b>	<b>1</b>
<b>2 Theoretical Background</b>	<b>5</b>
2.1 Grain growth in mesoscale . . . . .	5
2.1.1 General Review on Grain Growth Phenomena . . . . .	5
2.1.2 Abnormal Grain Growth . . . . .	7
2.2 Orientation representation . . . . .	10
2.2.1 Orientation Matrix . . . . .	10
2.2.2 Euler angles . . . . .	11
2.2.3 Angle/axis representation . . . . .	12
2.2.4 Rodrigues vector . . . . .	13
2.2.5 Misorientation representation . . . . .	13
2.3 Phase field method . . . . .	14
<b>3 Model Extension</b>	<b>19</b>
3.1 Simplified Model . . . . .	19
3.1.1 Effect of $\kappa$ parameter on the boundary energy . . . . .	23
3.1.2 Effect of $\gamma$ parameter on the boundary energy . . . . .	24
3.1.3 Effect of $m$ parameter on the boundary energy . . . . .	25
3.1.4 Effect of parameters combination . . . . .	25
3.2 Resolving the difficulties of the simplified model . . . . .	28
3.2.1 Effect of model parameters on the interfacial profiles . . . . .	30
3.2.2 Grain boundary energy . . . . .	32
3.2.3 Anisotropic grain boundary properties . . . . .	32
3.2.4 Misorientation-dependent model parameters . . . . .	34
<b>4 Results</b>	<b>37</b>
4.1 Implementation of the algorithm for obtaining the mis-orientation-dependent model parameters . . . . .	37
4.2 Two-dimensional anisotropic simulation results . . . . .	41
4.3 Three-dimensional anisotropic simulation results . . . . .	44
4.3.1 Anisotropic Energy and Constant Mobility . . . . .	45
4.3.2 Anisotropic Mobility and Constant Energy . . . . .	47

4.3.3	Anisotropic Energy and Anisotropic Mobility . . . . .	47
<b>5</b>	<b>Discussion</b>	<b>53</b>
5.1	Qualitative Analysis . . . . .	53
5.1.1	Shifting cutoff misorientation to higher values . . . . .	53
5.1.2	Experimenting with different values of energy plateau . . . . .	56
5.1.3	Contribution from the anisotropic mobility . . . . .	56
5.2	Quantitative comparison between the normal and abnormal grain growth models . . . . .	59
<b>6</b>	<b>Summary and Outlook</b>	<b>67</b>
	<b>Bibliography</b>	<b>69</b>

# Chapter 1

## Introduction

Grain growth is the last stage of annealing process coming after recovery and recrystallization. It is the process of microstructure evolution resulting in the increase of the grain size and is driven by the reduction of the grain boundary energy. Grain size control is an important part of the materials production and characterization [1]. The significance of this process comes from the fact that many mechanical properties of polycrystalline materials depend on the grain size distribution.

Earlier by our group a Al-1 wt.% Mg sample was investigated by the 3DXRD experiment in Japan. The reconstructed microstructure at different time steps are shown in Figure 1.1.

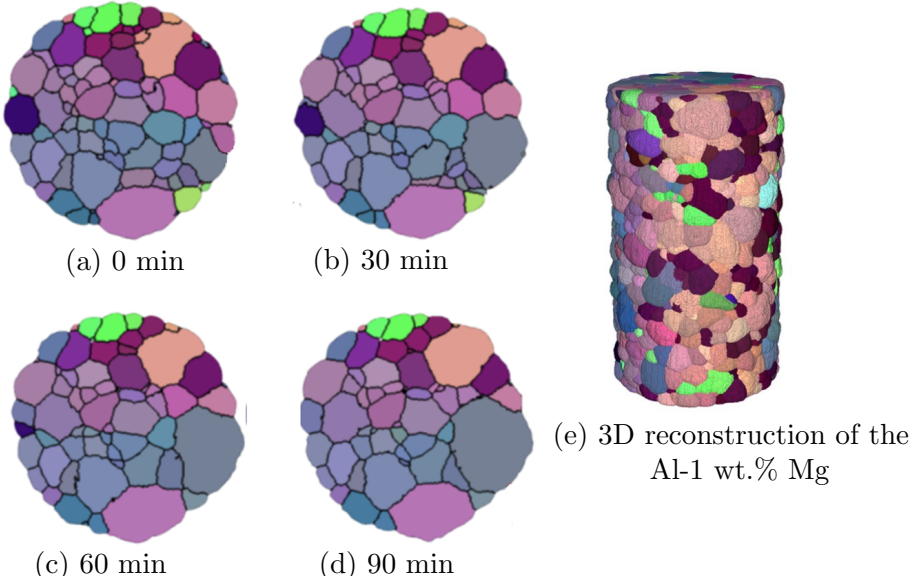


FIGURE 1.1: Microstructure evolution on slice 40 of a 3D reconstruction of a Al-wt.% Mg at different annealing time at 400°C, (a)-(d) . 3D reconstruction image of the whole sample. Measurements were done at the SPring-8 synchrotron, Japan, (e).

There are two types of grain growth that can be observed during annealing process: normal and abnormal grain growth [2]. First one is characterized by uniform increase of the grain sizes, while during the second one some grains grow at a significantly higher growth rate than the rest of the grains, leading to the situation when few grains are extremely big and others are small.

First attempt was done to predict the experimental microstructure by performing the normal grain growth simulation. Comparison between the experimental results and simulation results is provided in Figure 1.2.

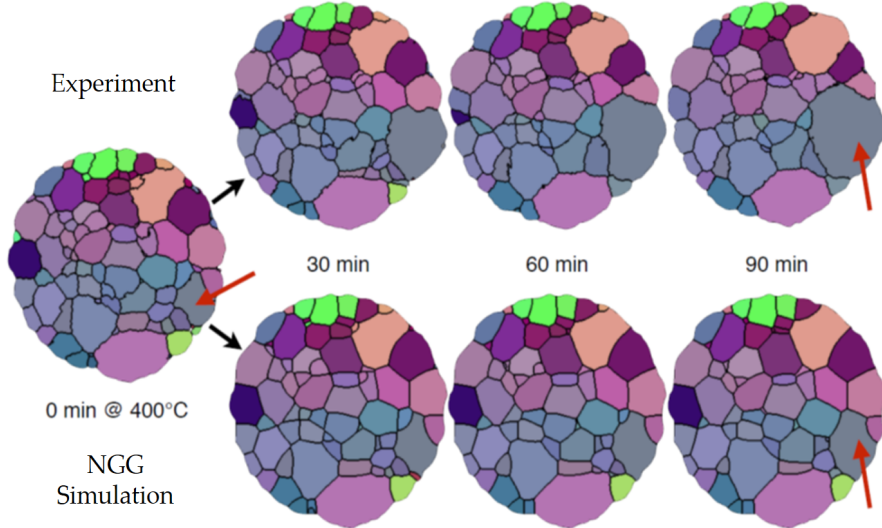


FIGURE 1.2: Comparison between the experimental results and the normal grain growth (NGG) prediction. Grain marked with red arrow proves the inconsistency of the isotropic model, according to which all grain boundaries have the same energy and mobility.

Taking closer attention to the comparison it can be noticed that the majority of the grains come with a quite good match with experimental results, but in the simulation some of the grains, like the one shown with the red arrow, couldn't achieve similar size as the experimental one. From these results it can be concluded that the normal grain growth simulation cannot describe what was happening during the experiment.

One of the possible explanations of the abnormal grain growth phenomenon is anisotropic nature of grain boundary energy,  $\sigma_{gb}$ , and mobility,  $\mu_{gb}$ , as opposed to the constant values in case of normal grain growth. Anisotropy comes from the misorientation between the neighboring grains. When misorientation  $\theta < \theta_m$ , grain boundary is called low-angle grain boundary and when  $\theta > \theta_m$ , high-angle grain boundary, where  $\theta_m$  is called a cutoff misorientation [3]. Typical value for cutoff misorientation is  $\theta_m = 15^\circ$  [2].

Phase-field method is a widely used instrument for predicting microstructure evolution, which incorporates physical values of the model through phenomenological parameters.

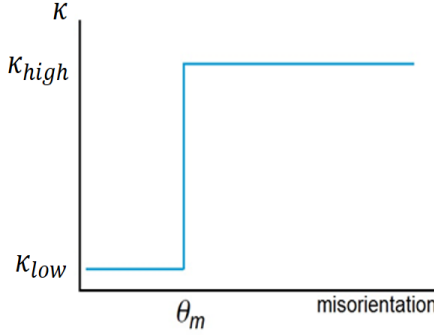


FIGURE 1.3: Step behavior of  $\kappa$ , phenomenological parameter used in the phase field method. It is known to affect the grain boundary energy.

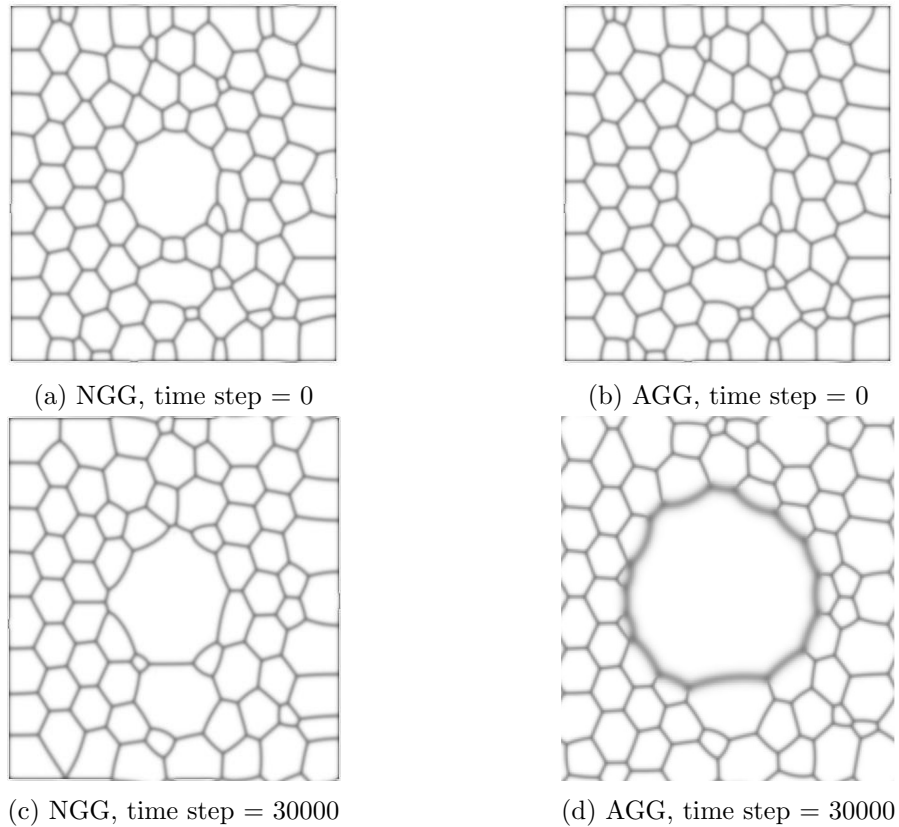


FIGURE 1.4: Simulation of the artificial microstructure for 30000 steps. Normal grain growth results, (a) and (c). Abnormal grain growth with implemented step behavior of  $\kappa$  parameter, (b) and (d).

As a first step it was decided to use a very simplistic approach – to use the step function for the phenomenological parameter  $\kappa$  (Figure 1.3), then perform phase field simulation and see how it affects the microstructure evolution. The artificial microstructure, which is simply a big grain surrounded with grain matrix of smaller grains, was investigated under the condition of grain boundaries for the bigger grain being high-angle and therefore higher energy. Figures 1.4 (a), (c) show the results from normal grain growth of such a structure and Figure 1.4 (b), (d) results of anisotropic approach, respectively.

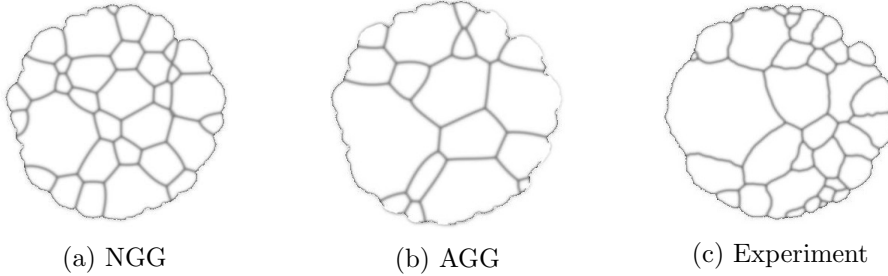


FIGURE 1.5: Simulation results of the two-dimensional microstructure captured from slice 430. Results on (a) and (b) are showing the microstructure for the normal and abnormal grain growth respectively. Comparison can be done with the experimental result (c).

Comparing these two pictures it can be concluded that grain growth under anisotropic condition can have significant impact on the resulting microstructure. Later investigation was done for the two-dimensional microstructure, which is a slice from the real sample, showing some noticeable influence to the simulation result from anisotropic growth (Figure 1.5).

In consideration of these results I hypothesize that experimental results for 3D grain growth can be modeled more accurately by introducing misorientation-dependent grain boundary properties into simulation algorithm. In the following chapters investigation of this hypothesis would be discussed. Starting from Chapter 2, the needed theoretical background is introduced, which is followed then with Chapter 3 containing details about the anisotropic model. Chapter 4 and Chapter 5 shows the investigations and conclusions regarding the above mentioned hypothesis. Chapter 6 summarizes the results of this thesis work.

# Chapter 2

## Theoretical Background

### 2.1 Grain growth in mesoscale

#### 2.1.1 General Review on Grain Growth Phenomena

Crystalline solids are constructed as a result of periodic repetition of the certain arrangement of atoms called unit cells. If this process is not interrupted, the result is called a single crystal. Single crystals can be found in nature and also can be grown in the special laboratories [1]. Most of crystalline solids are not single crystals, but composed of a big amount of small crystals which are called grains and such materials called polycrystalline [1]. Grains stay in contact with each other and have different crystallographic orientations. Transition from one grain to another is going through a narrow region between adjacent grains which is called a grain boundary.

Strengthening techniques involve plastic deformations into material which eventually leads to the excess energy stored in the material [1]. After that to make a material again more workable and reduce its hardness, annealing treatment should be applied. Annealing is a heat treatment process consisting of three stages: recovery, recrystallization and grain growth [2].

During recovery, atomic diffusion is increased which leads to the motion of dislocations. Dislocation motion allows the material to relieve internal stresses and eventually become softer. Recrystallization process is described by the nucleation of strain-free grains and subsequent growth until parent grains are consumed. The last stage of the annealing process is the grain growth. When keeping the specimen at high enough temperature, grains which started growing during the recrystallization, continue growth process and therefore reduce total area of grain boundaries. Grain boundary is a crystal defect,

which means that it has some excess free energy. Therefore by reducing the total grain boundary area, total energy is reduced. So the driving force for the grain growth is the reduction of energy which is stored in the form of grain boundaries.

Mechanical properties of materials depend on the grain size and therefore it is of industrial importance to control the grain growth process in order to achieve the desired effects [4]. When grains are of smaller size, they act as obstacles to dislocation slip and therefore produce the strengthening effect. Opposite result appears when the grains are of bigger size, then the material becomes softer.

Burke and Turnbull [5] derived the kinetics of the grain growth, in which the driving pressure on the boundary ( $\mathbf{P}$ ) is affected only by the curvature of the boundary and can be written as

$$P = \sigma_{gb} \left( \frac{1}{R_1} + \frac{1}{R_2} \right), \quad (2.1)$$

where  $\sigma_{gb}$  is the grain boundary energy and  $R_1$  and  $R_2$  are the principal radii of grain curvature. Burke and Turnbull assumed that  $\sigma_{gb}$  is the same for all the grain boundaries and averaged over whole ensemble of grain boundaries and got the following expression:

$$\bar{P} = \frac{\alpha \sigma_{gb}}{\bar{R}} \quad (2.2)$$

where  $\alpha$  is a geometric constant. Because velocity of the boundary  $v_{gb} = \frac{dR}{dt}$  is proportional to the pressure  $\mathbf{P}$ , then it can be obtained that

$$\bar{R}^2 - \bar{R}_0^2 = ct \quad (2.3)$$

where  $c$  is a constant. It was shown that this constant is proportional to the  $\mu_{gb}\sigma_{gb}$ , where  $\mu_{gb}$  is the grain boundary mobility[6]. The more general case is written as

$$\bar{R}^n - \bar{R}_0^n = ct \quad (2.4)$$

and the  $n$  is called the grain growth exponent and in theoretical considerations is equal to 2.

There are two types of grain growth that can be observed during the annealing process: normal grain growth and abnormal grain growth [2]. Normal grain growth is a continuous process (Figure 2.1 (a)) characterized with uniform increase of the size of the grains and

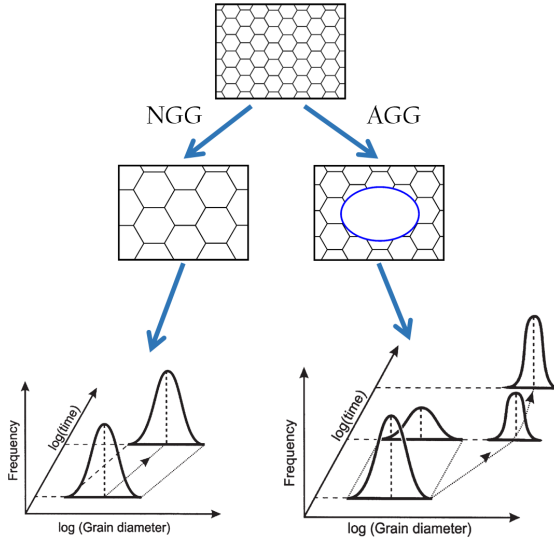


FIGURE 2.1: Normal grain growth (NGG) is a process where the shape of the grain size distribution will not change with time. Abnormal grain growth (AGG) is a process of growth, where few grains obtain the growth rate domination over other grains and give bimodal distribution followed with the unimodal of larger size grains. Adapted from [2] and Wikipedia [8].

quasi-stationary size distribution. During normal grain growth larger grains become bigger, consuming the smaller size grains, but the distribution of grain sizes scaled over the average grain size for the normal grain growth remain self-similar. This time-independent behavior generally takes lognormal shape [7].

Abnormal grain growth is characterized by a situation when some grains obtain larger growth rate than the rest matrix of grains and due to this consume many smaller grains, therefore becoming extremely big [2] (Figure 2.1 (b)). Instead of unimodal, as in case of normal grain growth, the size distribution becomes bimodal with further switch again to normal grain growth mode after all normal grains are consumed.

### 2.1.2 Abnormal Grain Growth

Reduction of total excess energy is the same driving force for abnormal grain growth as for normal grain growth. Preferential growth rate of some grains characterizes the grain growth to be abnormal.

One of the most famous example of material where the abnormal grain occurs is Fe-3% Si [9]. It is first observed by Goss in 1935 and still there is no clear explanation of this phenomenon. Electrical steels, also called Goss steels, are used in electrical transformers and control of the AGG allows to reduce the losses [2]. Examples of observation of the abnormal grain growth in the real material is shown in Figure 2.2.

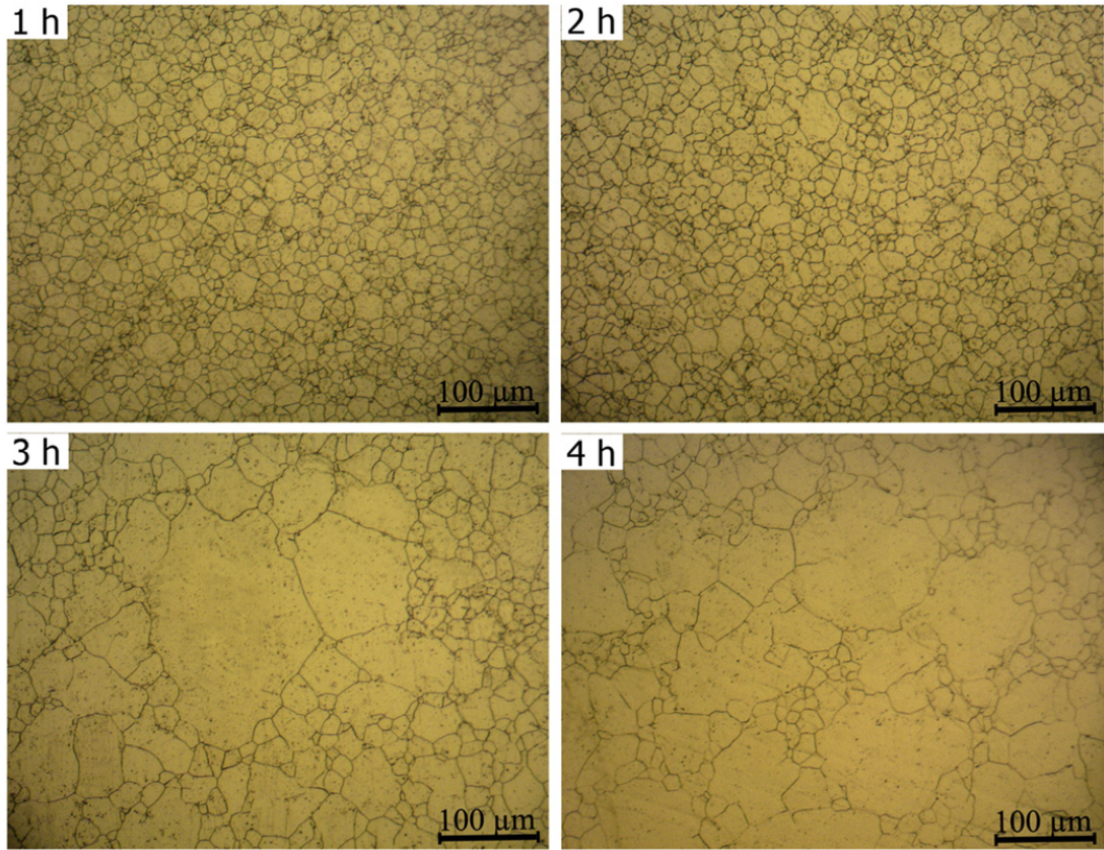


FIGURE 2.2: Abnormal grain growth in AISI 304L austenitic stainless steel during annealing at 850°. Figure from [10].

The complete theory which can explain the nature of the abnormal grain growth is still not developed, but there are some factors studied, which usually provoke the abnormal grains to occur. Those are second-phase particles pinning (Zener pinning), texture of the material and solid-state wetting [2].

Real materials usually contain some small amount of second-phase particles which can be precipitates or insoluble material. These particles provoke the pinning effect on the grain growth process [11]. It is also called Zener pinning, because he was the first who proposed a quantitative theory. Second-phase particles tend to decrease the mobility of the grain boundaries thus suppressing the grain growth process. Recent studies showed that different approaches of solid-state wetting can also lead to abnormal grain growth. In particular, it was shown by Rollett et al. [12] that AGG can appear due to anisotropic energy as well as due to the anisotropic grain boundary mobility. They introduced a model of wetting as a process that when three grains are in contact, forming triple junction, the high-energy boundary is replaced with the two low-energy boundaries.

In polycrystalline materials distribution of the grain orientations is called texture [13]. If material has a random distribution of orientations, the material has no texture. Texture

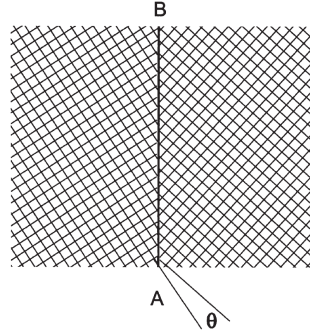


FIGURE 2.3: Two crystallites of different orientation, when coming into contact, form a grain boundary. Misorientation angle is denoted with  $\theta$  symbol.

can be observed in many materials and has a great impact on the properties of the materials [14]. Presence of the texture during annealing process leads to the abnormal grain growth and was discovered in many different materials like aluminum, copper and others [15–17].

Grain boundaries play an essential role in the AGG phenomenon. Schematic representation of the grain boundary is shown in Figure 2.3.

The grain boundary can be set by 5 degrees of freedom. Two degrees of freedom are coming from the rotation of the plane **AB** relative to one of the grains, called inclination and the rest three are required for the smallest rotation ( $\theta$ ) that will make crystallographic planes coincident and called misorientation. In most cases dependence on inclination can be neglected and only misorientation is considered [18]. Different ways of defining the misorientation are introduced in the next section.

There is some certain angle of misorientation which is usually around  $15^\circ$  that is called cutoff misorientation [3], which defines two types of grain boundaries. If misorientation is greater than this value, then the boundary is called high angle and if smaller, low angle grain boundary. Physical reason to such a division lies in the fact that low angle grain boundaries are dislocation arrays and their properties depend on the misorientation, while the high angle grain boundaries mostly do not depend on the misorientation [3]. Energy for low angle grain boundaries was derived by Read and Shockley [3] and the relation looks the following

$$\sigma = \begin{cases} \sigma_m \frac{\theta}{\theta_m} \left(1 - \ln \frac{\theta}{\theta_m}\right) & \text{for } \theta \leq \theta_m \\ \sigma_m & \text{for } \theta > \theta_m \end{cases} \quad (2.5)$$

where  $\theta_m$  is cutoff misorientation and the  $\sigma_m$  is the value of energy for high angle boundaries, so-called energy plateau.

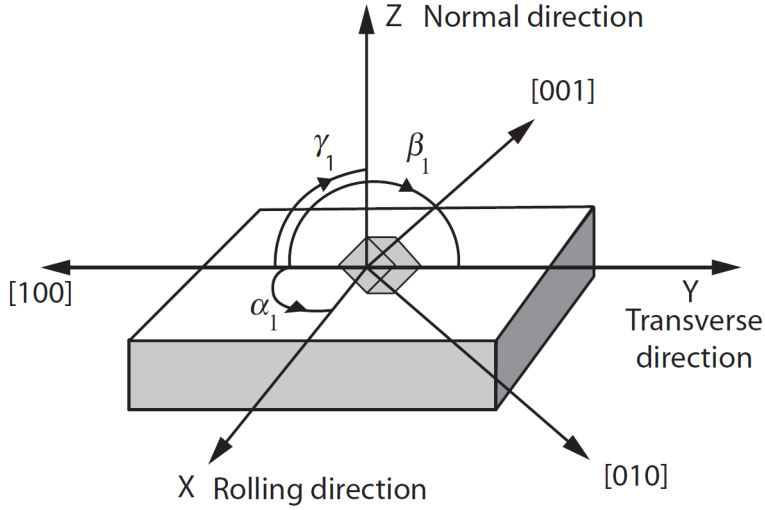


FIGURE 2.4: Specimen coordinate system XYZ(RD, TD, ND) and coordinate system for the crystal 100,010,001.  $\alpha_1$ ,  $\beta_1$ ,  $\gamma_1$  are angles between the 100 and XYZ axes, giving the first row of the orientation matrix.

## 2.2 Orientation representation

Term *orientation* expresses a definition of the crystal in space. But these coordinates exist only relative to some reference. Therefore to define an orientation, two coordinate systems are needed: one for the whole sample, which plays a role of the reference system, and another one of the crystal itself. Reference coordinate system should be chosen according to the external shapes of the sample. If the material is fabricated in terms of rolling, coordinate system axes are assigned according to the Rolling Direction (RD), direction normal to the rolling plane (ND) and the transverse direction (TD) (Figure 2.4).

Choice of the crystal coordinate system can be arbitrary, but usually is taken according to the symmetry of the crystal, made orthogonal and normalized.

### 2.2.1 Orientation Matrix

When specimen and crystal coordinate systems are assigned, the orientation is then defined as a matrix  $g$ , which is connected with the crystal ( $C_C$ ) and specimen ( $C_S$ ) coordinate systems in the following way:

$$C_C = g \cdot C_S, \quad (2.6)$$

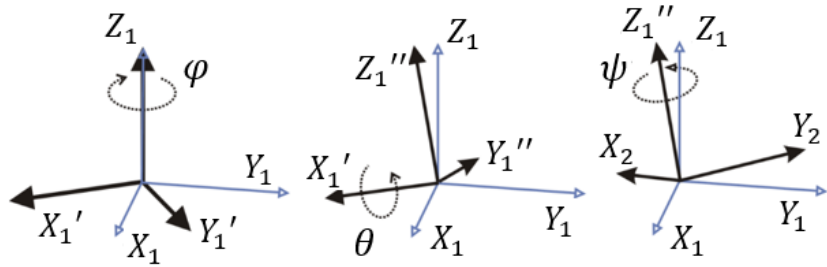


FIGURE 2.5: Representation of the coordinate systems and corresponding angles bringing  $X_1Y_1Z_1$  coordinate system to  $X_2Y_2Z_2$  one. Adapted from Wikipedia [19].

Orientation matrix consists of three rows with three elements, where each row can be obtained by taking every axis of the crystal coordinate system and calculating the cosines of the angles between the crystal axis and specimen axes, X, Y, Z. Thus, the matrix gets the following expression:

$$g = \begin{pmatrix} \cos\alpha_1 & \cos\beta_1 & \cos\gamma_1 \\ \cos\alpha_2 & \cos\beta_2 & \cos\gamma_2 \\ \cos\alpha_3 & \cos\beta_3 & \cos\gamma_3 \end{pmatrix} = \begin{pmatrix} g_{11} & g_{12} & g_{13} \\ g_{21} & g_{22} & g_{23} \\ g_{31} & g_{32} & g_{33} \end{pmatrix} \quad (2.7)$$

Figure 2.4 explains the set of angles.

There are different ways in which the orientation can be represented.

### 2.2.2 Euler angles

Euler representation consists of three rotation angles, which should be applied in proper sequence to the specimen coordinate system to coincide it with the crystal one. There are certain rules for these angles:

- 1)  $\phi$  - is the angle of rotation about the  $Z_1$  axis, bringing the  $X_1$  and  $Y_1$  axes to  $X_1'$  and  $Y_1'$  respectively
- 2)  $\theta$  - is the angle about the  $X_1'$
- 3)  $\psi$  - is the angle about  $Z_1''$

All three angles and rotation operations are shown in Figure 2.5.

Transformation between the rotation matrix and the Euler angles can be done through these relations [13]:

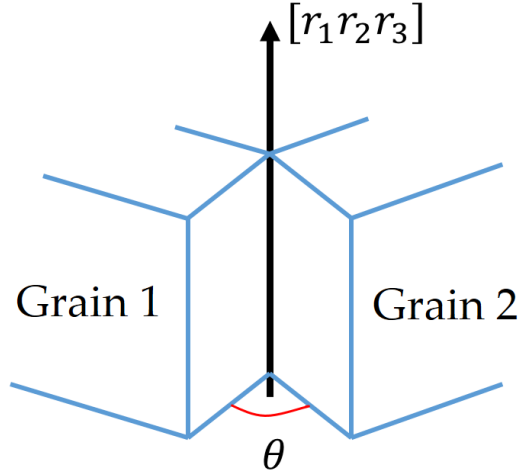


FIGURE 2.6: Angle/axis description of the misorientation between two adjacent grains.

$$\begin{aligned}
 g_{11} &= \cos\varphi \cos\psi - \sin\varphi \sin\psi \cos\theta \\
 g_{12} &= \sin\varphi \cos\psi + \cos\varphi \sin\psi \cos\theta \\
 g_{13} &= \sin\psi \sin\theta \\
 g_{21} &= -\cos\varphi \sin\psi - \sin\varphi \cos\psi \cos\theta \\
 g_{22} &= -\sin\varphi \sin\psi + \cos\varphi \cos\psi \cos\theta \\
 g_{23} &= \cos\psi \sin\theta \\
 g_{31} &= \sin\varphi \sin\theta \\
 g_{32} &= -\cos\varphi \sin\theta \\
 g_{33} &= \cos\theta
 \end{aligned} \tag{2.8}$$

### 2.2.3 Angle/axis representation

Another approach allowing to translate the crystal systems one to another is to rotate only once but through a special axis. This approach is also called angle/axis representation (Figure 2.6). Conversion between the rotation matrix approach and angle/axis one is following [13]:

$$\begin{aligned}
 \cos\theta &= \frac{g_{11} + g_{22} + g_{33} - 1}{2} \\
 r_1 &= \frac{g_{23} - g_{32}}{2\sin\theta} \\
 r_2 &= \frac{g_{31} - g_{13}}{2\sin\theta} \\
 r_3 &= \frac{g_{12} - g_{21}}{2\sin\theta}
 \end{aligned} \tag{2.9}$$

where  $\theta$  is the rotation angle about the rotation axis  $[r_1 r_2 r_3]$  in reference coordinate system.

#### 2.2.4 Rodrigues vector

Another way for representing orientations is Rodrigues vector. It is based on the angle/axis approach, and like Euler angles, consists of three independent variables. Rodrigues vector is defined as a combination of the angle and axis information in one vector:

$$R_i = \tan\left(\frac{\theta}{2}\right) \cdot r_i, i = 1, 2, 3 \tag{2.10}$$

The main advantage of this approach is that components of the Rodrigues vector can be used to map the orientations in color and make it able to distinguish easily different grains that are present in the microstructure.

#### 2.2.5 Misorientation representation

Rotation between two crystallites is called misorientation. For example, if rotation from orientation  $g_2$  to  $g_1$  should be done, then they would be connected through following relation:

$$g_1 = M_{12} \cdot g_2 \tag{2.11}$$

$$M_{12} = g_1 \cdot g_2^{-1} \tag{2.12}$$

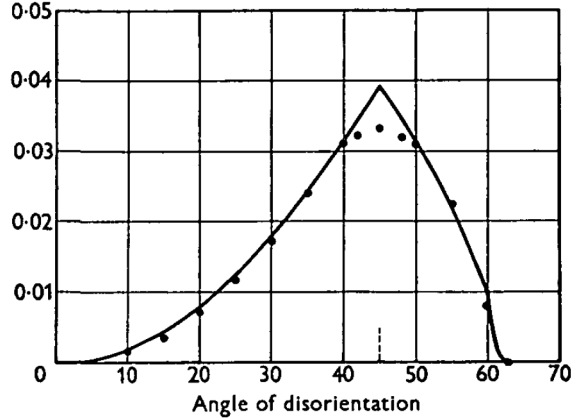


FIGURE 2.7: Mackenzie distribution of the misorientation angles in the sample which obeys the random texture [20].

$M_{12}$  is the misorientation matrix. The misorientation is often described by the rotation angle from the angle/axis representation, because the axis is usually not involved into the discussion of the boundary properties [18].

If a material with cubic lattice symmetry has a random texture, then misorientations follow a certain distribution, called Mackenzie distribution, which has a maximum at  $45^\circ$  and is limited with the misorientation equal to  $62.8^\circ$  [20] (Figure 2.7).

Because of the symmetry there are many ways in which the misorientation can be specified. Usually the smallest value is considered and according to a special algorithm [21] it can be obtained through the following expression:

$$\phi = \arccos\left(\max_j \text{Tr}(g \cdot S_j) - 1\right)/2 \quad (2.13)$$

where  $g$  is the orientation matrix,  $S_j$  stands for the matrices of the 24 symmetrical operations like: identity, rotations of  $180^\circ$  around three  $<100>$  axes, rotations of  $90^\circ$  about the same axes, rotations of  $180^\circ$  around the six  $<110>$  axes and rotations of  $120^\circ$  around the four  $<111>$  axes [21].

## 2.3 Phase field method

Experimental studies of the grain growth can be difficult in terms of time and control. Simulation is a perfect instrument for a researcher, allowing to get fast and physically-consistent results. For the mesoscale simulations, that predict the microstructure evolution, there are several possible techniques that can be used. Monte Carlo [22], vertex

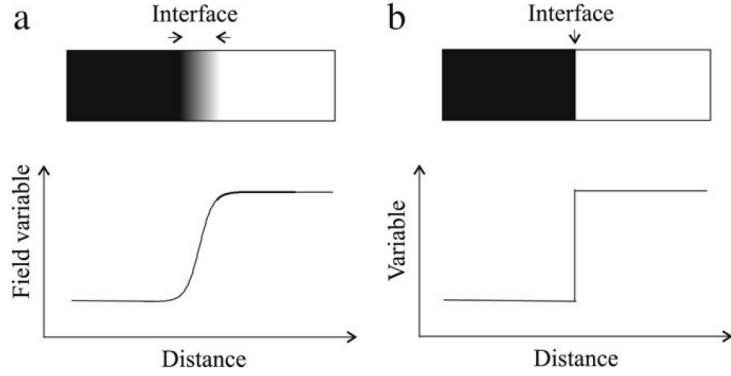


FIGURE 2.8: Different interface representation. Left image is for diffuse one and to the right is the sharp interface approach. From [30].

[23], cellular automata [24] and phase field method [25] are the ones that used mostly for the microstructure prediction.

Grain boundaries in material is a transition region between the grains having different crystallographic orientations. Therefore the density of the atoms varies from the bulk region to the grain boundary region. Such a system is called being 'nonuniform'. Cahn and Hillard [26] derived a theory for such nonuniform systems. It was assumed the existence of the free energy for homogeneous part of the material, which is a function of the long-range order parameter  $\eta$ . This parameter can represent any real physical value like density or composition.

Free energy is a result of two contributing parts, one is the homogeneous part and another is the gradient part [26]. For grain growth in metals the grain boundary is the region where the atom rearrangement happens and diffusion is required. It was shown by Allen and Cahn [27] that diffusion in grain boundaries can be explained with the gradient parts of the free energy and it leads to the translation of the boundary eventually. This diffuse-interface model was used by Chen and Yang [28] in order to simulate the microstructure of grains with different crystallographic orientations, by using a set of order parameters so that grains can be distinguished. Later additional restriction on the order parameters was added that  $\sum_i \eta_i = 1$ , representing the volume fraction of each grain at a certain point [29]. This multiorder parameter representation of the systems with the following application of the kinetic equation is called phase-field method.

Opposite to the diffuse-interface model, other simulation techniques, for example Monte Carlo Potts model, are using the sharp representation of the interface (Figure 2.8).

Sharp-interface approach can be used mostly to one-dimensional systems or simplistic grain microstructures [30]. For the diffuse interfaces kinetic equations can be applied to

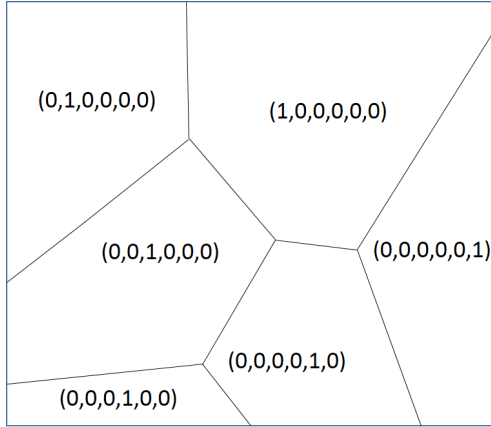


FIGURE 2.9: Grains microstructure assigned with order parameters. Every single grain can have only one non-zero value. Number of parameters is equal to the number of grains.

the whole system and evolution of complex grain structures can be simulated. Another advantage of diffuse approach is that the grain boundaries need not be tracked during the microstructure evolution.

In phase field method set of continuous functions  $\eta_i(\mathbf{r}, t)$ , also called order parameters, depending on the spatial coordinates and time, are introduced. It was shown [31], that the evolution of the microstructure is greatly affected by the amount of order parameters used for the simulation process. When the number of order parameters is less than the initial amount of grains it is very possible that the coalescence will happen. Coalescence is an event when during the simulation two grains with the same assigned orientation come into contact with each other, resulting in the merge of these grains. In order to avoid this artifact, Fan and Chen [32] suggested approach which takes the number of order parameters equal to the number of grains in the initial microstructure.

These functions are defined in such a way that within the bulk of a certain grain  $i$ , the  $i$ th order parameter is equal to 1 and all other order parameters are zero (Figure 2.9). Within the interface region order parameters vary smoothly and this diffusive transition of order parameters between the grains makes it possible for grain boundaries to move without the need to be tracked (Figure 2.10). The evolution of these order parameters is expressed by the Ginzburg Landau equation:

$$\frac{\partial \eta_i}{\partial t} = -L \frac{\delta F}{\delta \eta_i} \quad (2.14)$$

where  $L$  is a kinetic coefficient and  $F$  is a free energy of the whole system. Free energy is usually a sum of different contributions responsible for the microstructural evolution.

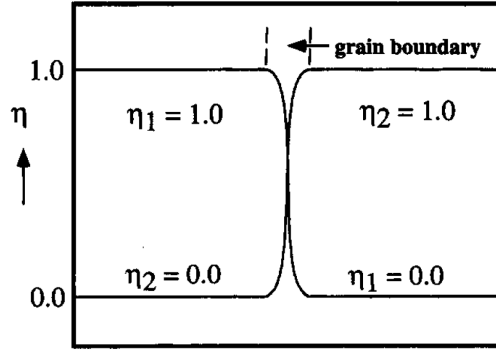


FIGURE 2.10: Behavior of the order parameters at the interface. Diffuse change from 1 to 0 is the region of the grain boundary. From [32].

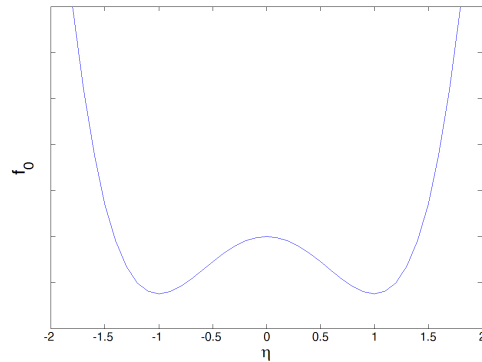


FIGURE 2.11: Free energy of the material as a function of long-range parameter  $\eta$ .

When there is no change of the temperature, pressure, molar volume and neither magnetic or electrical fields are applied, the main contributors to the free energy are bulk free energy and interface free energy. In such a case total free energy is given by

$$F = \int_V \left[ f_0(\eta_1, \dots, \eta_p) + \frac{\kappa}{2} \sum_{i=1}^p (\nabla \eta_i)^2 \right] dV, \quad (2.15)$$

where  $f_0$  is a homogeneous free energy that represents the bulk free energy and gradient parts are representing the interfacial free energy,  $\kappa$  is called gradient energy coefficient,  $p$  is the number of order parameters. Homogeneous free energy is constructed in such a way to provide large number of minimum values for the order parameters:

$$f_0(\eta_1, \dots, \eta_p) = \sum_{i=1}^p \left( -\frac{\alpha}{2} \eta_i^2 + \frac{\beta}{4} \eta_i^4 \right) + \sum_{i=1}^p \sum_{j>i}^p \gamma \cdot \eta_i^2 \eta_j^2 \quad (2.16)$$

The characteristic shape for this function for one order parameter is shown in Figure 2.11. All together  $\alpha$ ,  $\beta$ ,  $\gamma$ ,  $\kappa$  and  $L$  are called phenomenological parameters.

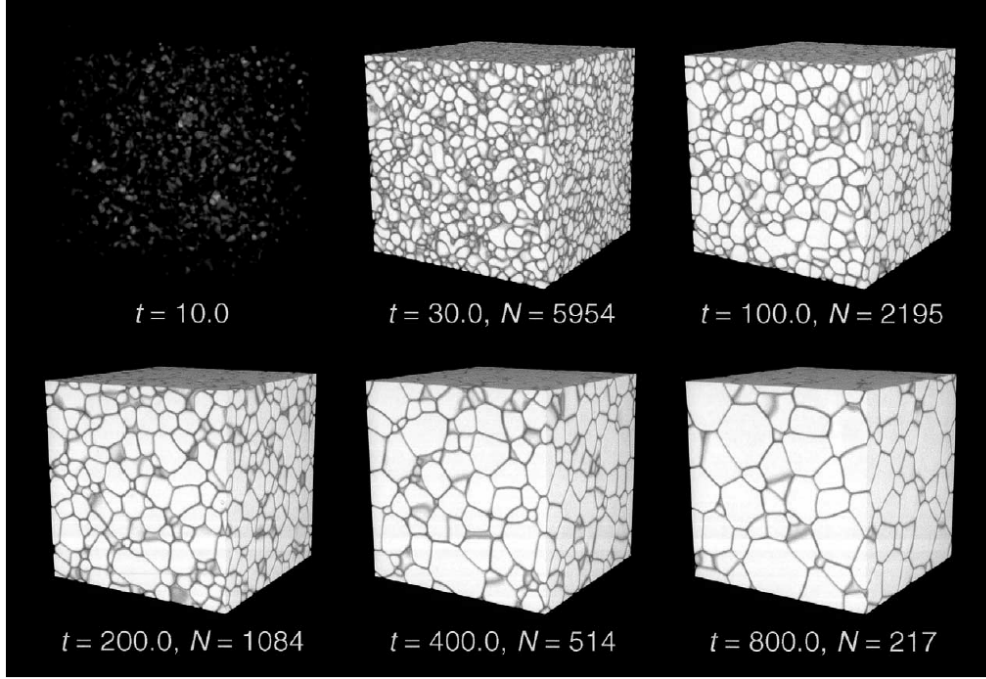


FIGURE 2.12: Three-dimensional phase-field simulation of the microstructure evolution. Starting microstructure is obtained through nucleation of the undercooled liquid.

From [33].

In order to solve Equation 2.14 numerically on the computer, it should be discretized. Using forward Euler equation for the left part and considering that derivative of the gradient part of the free energy expression gives the laplacian function, resulting equation that is used by computer code looks the following:

$$\frac{\eta_i(\mathbf{r}, t + \Delta t) - \eta_i(\mathbf{r}, t)}{\Delta t} = -L \left( -\alpha \eta_i(\mathbf{r}, t) + \beta \eta_i^3(\mathbf{r}, t) + 2\gamma \eta_i(\mathbf{r}, t) \sum_{j \neq i}^p \eta_j^2(\mathbf{r}, t) - \kappa \nabla^2 \eta_i(\mathbf{r}, t) \right) \quad (2.17)$$

and

$$\nabla^2 \eta_i(\mathbf{r}, t) = \frac{1}{(\Delta x)^2} \sum_i^{1nn} (\eta_i(\mathbf{r}_i, t) - \eta_i(\mathbf{r}, t)) \quad (2.18)$$

In Figure 2.12 example of the microstructural evolution with the phase-field method is shown for a crystal obtained from undercooled liquid.

Phase-field method can solve different variety of problems like grain growth simulation [28], dislocation dynamics [34], crack propagation [35] and electromigration [36].

# Chapter 3

## Model Extension

### 3.1 Simplified Model

Recalling back what was discussed in the introduction, the transformation of the phenomenological parameter  $\kappa$  from the constant value to the step function leads to a significant effect on the microstructure evolution as shown in Figure 1.5. Moreover, the investigation of the application of such an anisotropic model onto the real microstructure gives a deeper understanding that anisotropic behavior can play a significant role in the explanation of the grain growth in the experimentally studied sample.

But from the Equation 2.16, it can be seen that except  $\kappa$ , there are other phenomenological parameters like  $\gamma$ ,  $L$  and  $\alpha$  and  $\beta$ . Considering  $\alpha = \beta$ , equation can be rewritten as [37]:

$$mf_0(\eta_1, \dots, \eta_p) = m \left( \sum_{i=1}^p \left( -\frac{\eta_i^2}{2} + \frac{\eta_i^4}{4} \right) + \sum_{i=1}^p \sum_{j>i}^p \gamma \cdot \eta_i^2 \eta_j^2 + \frac{1}{4} \right), \quad (3.1)$$

where  $m$  is the phenomenological parameter, which is responsible for the depth of the potential well and additional term  $1/4$  is added to make the homogeneous free energy be equal to zero within grains.

Those parameters contribute to the Ginzburg-Landau equation which eventually describes the evolution of grains. It is important to note that Ginzburg-Landau equation describes the time-dependent evolution of the phenomenological order parameters and not the real physical values. The fundamental relation of physical parameters as was pointed in the background chapter is simply this formula:

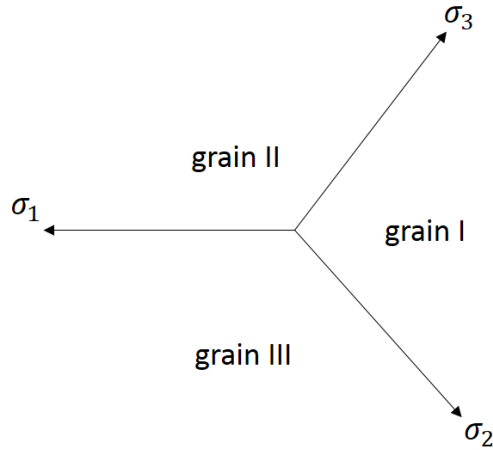


FIGURE 3.1: Triple junction structure

$$v_{gb} = \mu_{gb}\sigma_{gb}/R \quad (3.2)$$

Looking together at this expression and Ginzburg-Landau equation eventually leads to the idea that between physical values like grain boundary energy  $\sigma_{gb}$ , grain boundary mobility  $\mu_{gb}$  and phenomenological parameters like  $\kappa$ ,  $\gamma$ ,  $L$  and  $m$  should be some relation. From the original paper of Allen and Cahn [27] it is known that the grain boundary energy,  $\sigma_{gb}$ , is a function of  $\kappa$  parameter and mobility,  $\mu_{gb}$  is a function of the  $L$ .

But for the development of the sophisticated model it is essential to study how other parameters contribute to those values. Summarizing that it is of great importance to answer the question: how phenomenological parameters  $\kappa$ ,  $\gamma$ ,  $m$  and  $L$  contribute to the grain boundary energy and mobility.

When three grains coincide with each other we get a so-called triple junction structure which is shown in Figure 3.1. In order to get a minimal energy configuration, grain boundaries between adjacent grains make an angle of 120°. Mathematically it can be described by the so-called Young's law [38]:

$$\sum_i \vec{\sigma}_i = 0 \quad (3.3)$$

This law tells that the vector sum of all the energies contributing to the triple junction is zero.

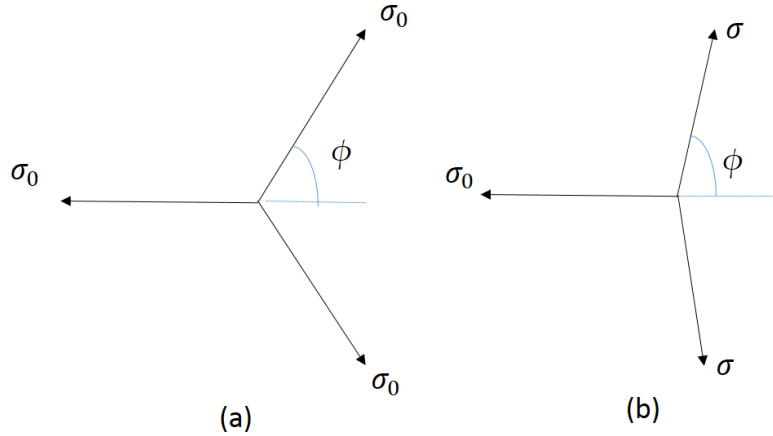


FIGURE 3.2: Triple junction structure with equal energies(a) and different energies(b)

In a specific case shown in Figure 3.2 (a), Young's law can be calculated as a projection of the energies of all the grain boundary energies on the axis which coincide with one of those energies:

$$\sigma_0 = 2\sigma_0 \cos\phi \quad (3.4)$$

As long as the isotropic nature of grain boundaries is considered, the energies for all three grain boundaries contributing to the triple junction are equal. This brings

$$\cos\phi = \frac{1}{2} \Rightarrow \phi = 60^\circ \quad (3.5)$$

As pointed out in the introduction part the case of isotropic energy was already studied and didn't bring sufficient results. It is interesting then to investigate how the same structure will look like for the case of anisotropic energy. Involving the anisotropic energy grain boundaries in the triple junction discussed above means that at least one of the energies would be different.

Considering the case with two boundaries having higher energy ( $\sigma > \sigma_0$ ), as shown in Figure 3.2 (b), the resulting Young's law would look like this:

$$\sigma_0 = 2\sigma \cos\phi \quad (3.6)$$

Bringing all the energy terms to one side leads to the following relation:

$$\frac{\sigma}{\sigma_0} = \frac{1}{2\cos\phi} \quad (3.7)$$

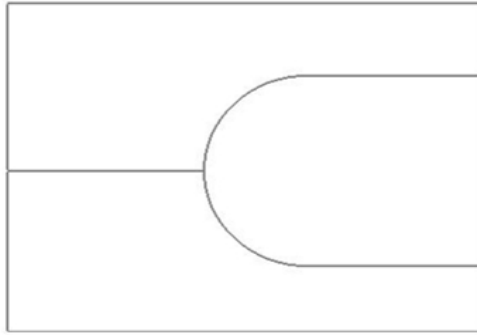


FIGURE 3.3: Initial microstructure

From the above relation it can be concluded, that if we can measure the angle in this given structure, we can get the ratio of grain boundary energies. According to this analysis the goal was set to develop such an artificial design of microstructure which can represent the triple junction and different energies could be assigned to the grain boundaries. Inspired by the work of Schvindlerman et al. [39] the model structure is shown in Figure 3.3.

This design should have been adapted for the purposes of obtaining the triple junction structure as a result of the microstructure evolution because the evaluation of the original design didn't show that it is able to reach a stable triple junction structure. The approach of making the ends of the two right grain boundaries fixed makes it possible to bring the dynamic evolution of such an artificial structure to the equilibrium state. At equilibrium state it is possible to obtain the values of angles and therefore, energy ratios can be obtained.

Coming to the second step of the process of investigating the effect of the phenomenological parameters on the energy and mobility of grain boundaries, the procedure should be discussed. The process of getting the closest match between the simulation results and experimental results requires a possibility of changing the phenomenological parameters in such a way that allows the simulation to give results which correspond to the results obtained by the experimental way. According to this, it is important to have sufficient range of parameters variation. That's why the procedure of investigating the phenomenological parameters consists of investigating individually every parameter's range on the energy and mobility. According to these results conclusions should be drawn if a certain phenomenological parameter does effect the energy and mobility or not and it should be concluded how the combination of parameters should be used in order to get certain range of desired grain boundary energies and mobilities.

In further chapters the process of development of simplified model is discussed. It is explained by examining each and every parameter how does it affect the energy of the

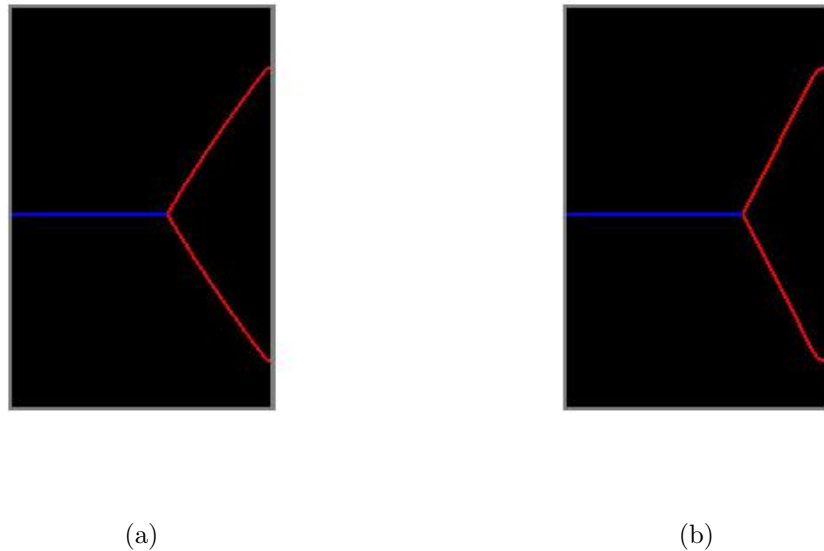


FIGURE 3.4: Artificial microstructure with high-angle boundaries (red) having value of  $\kappa=2.0$  (a) and  $\kappa=10.0$  (b), while  $\kappa$  for low-angle boundaries (blue) is equal to 2.0.

grain boundary.

### 3.1.1 Effect of $\kappa$ parameter on the boundary energy

The first parameter to be investigated is the  $\kappa$  parameter. But the first thing which should be done not only for this parameter but for other parameters also is validation of the results for the isotropic case. Meaning that assigning the same value of  $\kappa$  parameter to all three grain boundaries will give the angles with the angle of  $2\phi = 120^\circ$ . The following proof can be seen in the Figure 3.4 (a). The assigned value of  $\kappa$  is 2.0 for all grain boundaries.

Also from the above figure it can be noted that it was chosen the configuration consisting of two high-angle grain boundaries which are represented with the red color and one low-angle grain boundary represented with the blue color. The value of  $\kappa$  for low-angle grain boundary was fixed and was equal to 2.0. The value of  $\kappa$  for high-angle grain boundary was changed from 2.0 to 10.0 with a 0.5 step. Resulting values were normalized to the values of energy for the low-angle grain boundary as discussed before: In Figure 3.4b the resulting microstructure presented for the highest value of  $\kappa=10.0$ . The angle between two high-angle grain boundaries is  $2\phi = 128^\circ$ .

The resulting relation between the energy and  $\kappa$  parameter is shown in Figure 3.5. It can be seen that with increase of  $\kappa$  parameter, the energy is also increasing.

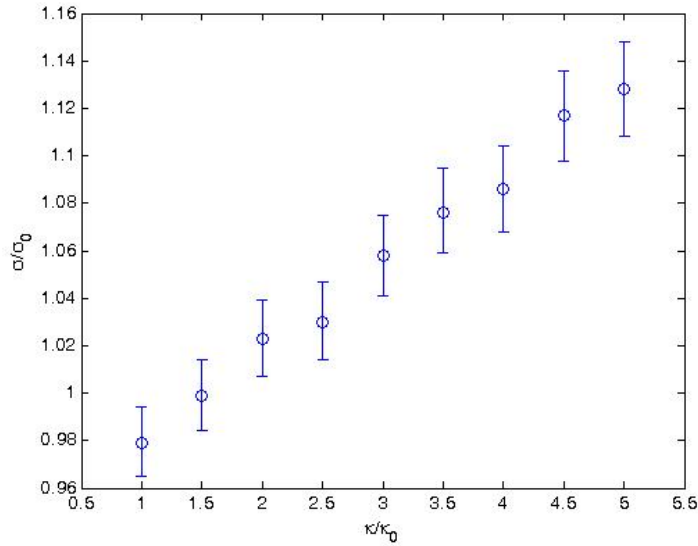


FIGURE 3.5: Dependence of the grain boundary energy ratio on the  $\kappa$  parameter.  $\kappa_0$  and  $\sigma_0$  correspond to the low-angle grain boundary.  $\kappa$  and  $\sigma$  correspond to high-angle grain boundary.

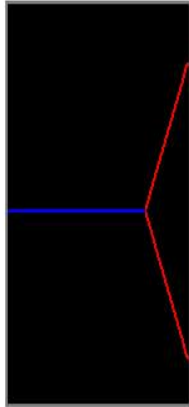


FIGURE 3.6: Artificial microstructure with high-angle boundaries (red) having value of  $\gamma=10.0$  and low-angle boundary (blue) had value equal to 1.0.

### 3.1.2 Effect of $\gamma$ parameter on the boundary energy

The next parameter that was studied was the  $\gamma$  parameter. The value for the low-angle grain boundary was  $\gamma_0=1.0$ . The maximum value for high-angle grain boundary that was investigated was  $\gamma=10.0$ . Figure 3.6 represents this case of microstructure. The observed angle is  $2\phi = 136^\circ$ .

Energy ratios as a function of  $\gamma/\gamma_0$  are shown in Figure 3.7 .

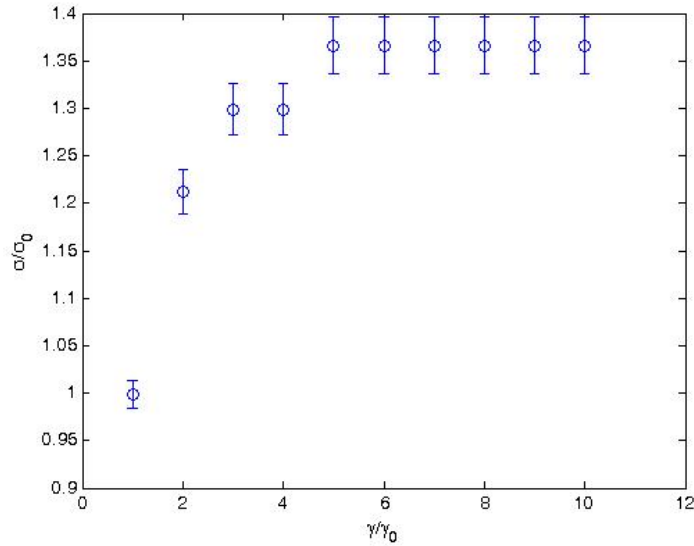


FIGURE 3.7: Dependence of the grain boundary energy ratio on the  $\gamma$  parameter.  $\sigma$  and  $\gamma$  correspond to high-angle grain boundaries.  $\sigma_0$  and  $\gamma_0$  were held constant and correspond to low-angle boundary.

From these results it can be stated that increase of  $\gamma$  parameter increases the value of energy. But comparing to the  $\kappa$  parameter it is not linear and comes to the plateau.

### 3.1.3 Effect of m parameter on the boundary energy

The last parameter investigated is the  $m$  parameter. This is the parameter with which the whole homogeneous free energy function is multiplied. This parameter is responsible for the depth of the potential well produced by free energy function. Low-angle grain boundary was assigned with  $m_0=1.0$  and the highest value for high-angle grain boundary was 8.0. The resulting microstructure for maximum value is shown in Figure 3.8 and the observed angle was  $2\phi = 71^\circ$ .

Effect of increasing  $m$  on the grain boundary energy ratio is shown in Figure 3.9. Increase of the  $m$  parameter follows with the decrease of the energy ratio.

It can be seen the opposite effect of this parameter on the grain boundary energy comparing to the  $\kappa$  and  $\gamma$ .

### 3.1.4 Effect of parameters combination

Studies provided above show how each phenomenological parameter can individually affect the energy. By varying one of the parameters certain range of desired values of energies can be obtained. Variation of energy for the needs of getting closer match of

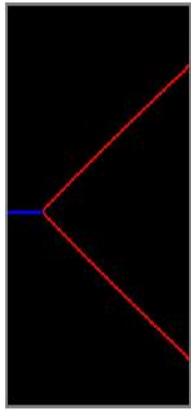


FIGURE 3.8: Artificial microstructure with high-angle boundaries (red) having value of  $m=8$ . Low-angle grain boundary (blue) has value of  $m$  equal to 1.0.

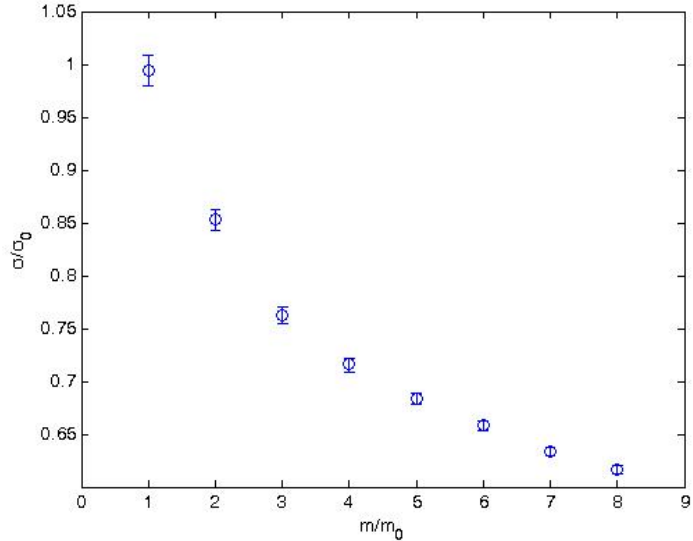


FIGURE 3.9: Dependence of the grain boundary energy ratio on the  $m$  parameter.  $\sigma$  and  $m$  correspond to high-angle grain boundaries and  $\sigma_0$  and  $m_0$  are constant values of low-angle grain boundary.

simulation results and experimental results should be provided with as much more values as possible. In other words the range of the energies used for the simulation matching should be as big as possible in order to provide sufficient freedom of microstructure variation. According to the results in the above sections only  $\kappa$  and  $\gamma$  make the grain boundary energy to increase with the increase of parameter. That's why it was decided to investigate the combination of the parameters  $\kappa$  and  $\gamma$  to see if their combination can provide even bigger values of grain boundary energies.

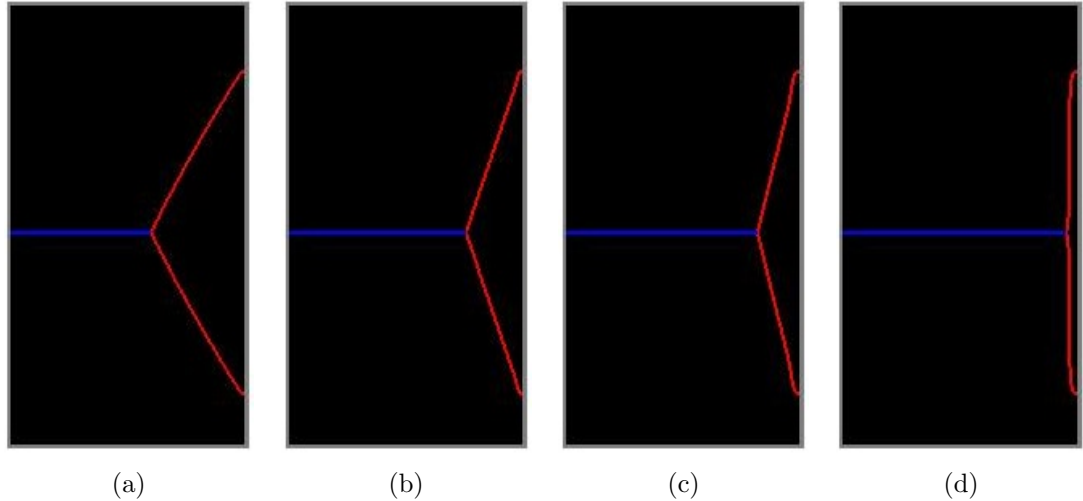


FIGURE 3.10: Artificial microstructure under influence of  $\kappa$  and  $\gamma$  parameter different values. Values are summarized in the Table below. For all cases values for low-angle grain boundaries are the following:  $\kappa_0 = 2.0$ ,  $\gamma_0 = 1.0$ .

Parameter \ Figure	a	b	c	d
$\kappa$	10	2	4	4
$\gamma$	1	10	2	3
$2\phi, {}^\circ$	128	136	150	162
$\sigma/\sigma_0$	1.14	1.33	1.93	4.75

For the same artificial microstructure used before different trial values of  $\kappa$  and  $\gamma$  were applied. Figure 3.10 shows the obtained results for the combination of parameters.

Cases a and b summarize the results obtained in the previous sections. Case a is responsible for the high-angle boundaries having highest value of  $\kappa$  and case b is responsible for the high-angle boundaries having highest value of  $\gamma$ . Case c is representing high-angle boundaries having both  $\kappa$  and  $\gamma$  being twice bigger than the value of the  $\kappa_0$  and  $\gamma_0$  for the low-angle grain boundary. It can be noticed that  $\kappa$  and  $\gamma$  individually are not even close to the maximum values studied before, but the combination of these two parameters provides the angle which is bigger comparing to the microstructure having maximum value of the either of those parameters. And for this case energy could be increased almost twice bigger. Doing some more research on these parameters variation it can be noticed that taking the case c and increasing the value, for example, of  $\gamma$  just by value 1.0 the observable angle is almost close to the  $180^\circ$  and change of energy is as big as 5 times. It can be concluded from these results that combination of parameters provides wider range of desired grain boundary energies comparing to the individual variation of  $\kappa$  or  $\gamma$  parameter.

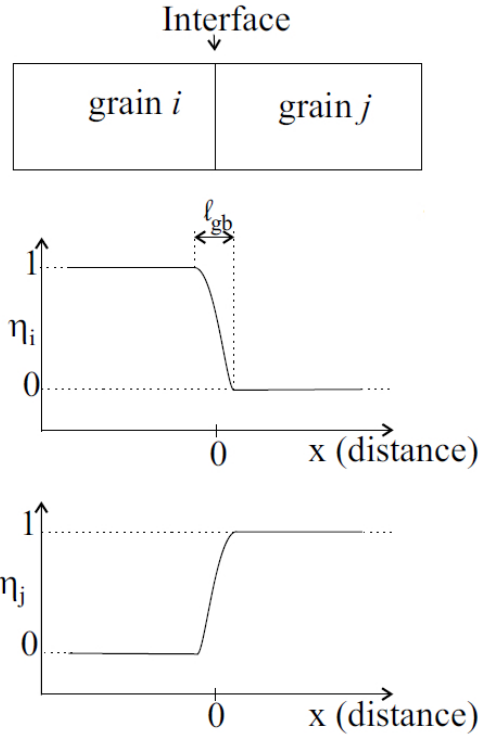


FIGURE 3.11: Simple two-grain structure representing two phase field variables  $\eta_i$  and  $\eta_j$ .  $l_{gb}$  is a length of grain boundary region. From [37].

### 3.2 Resolving the difficulties of the simplified model

Analyzing results shown in the previous sections it can be seen that for the case of energy it is dependent not only on a single parameter. Studied influence of  $\gamma$  parameter showed that energy can have more complicated relation between the phenomenological parameters and which cannot be studied with the simplified procedure previously suggested. According to this, more detailed research was required to investigate the more sophisticated relation between energy, mobility and phenomenological parameters.

A detailed study of phase field model in application to anisotropic systems has been discussed by Moelans [37]. In this section, theoretical overview of this quantitative analysis discussed in that article will be provided in a concise way.

Relations between model parameters and grain boundary energy can be derived from considering the simplistic structure consisting of only two grains shown in Figure 3.11.

The derivation is done under assumption that the interface between grains is flat and is in equilibrium. According to Equation 3.1, every grain boundary is characterized by parameters  $m$ ,  $\gamma_{i,j}$  and  $\kappa_{i,j}$ . Following the original work done by Cahn and Hilliard [26], grain boundary energy can be written by the following form:

$$\sigma_{i,j} = \int_{-\infty}^{+\infty} \left\{ m f_0(\eta_i, \eta_j) + \frac{\kappa_{i,j}}{2} \left[ \left( \frac{d\eta_i}{dx} \right)^2 + \left( \frac{d\eta_j}{dx} \right)^2 \right] \right\} dx, \quad (3.8)$$

where  $x$  here is the spatial coordinate which is normal to the grain boundary surface. Interface profiles  $\eta_i(x)$  and  $\eta_j(x)$  take such a shape to minimize the grain boundary energy.

According to the theory of calculus of variations the functional of the form  $F[u] = \int_{x_1}^{x_2} L[x, u(x), u'(x)] dx$ , substituted into the Euler-Lagrange equation  $\frac{\partial F}{\partial u} - \frac{d}{dx} \frac{\partial F}{\partial u'} = 0$  gives the minimized solution. Therefore following equations are obtained

$$m \frac{\partial f_0}{\partial \eta_i} - \kappa_{i,j} \left( \frac{d^2 \eta_i}{dx^2} \right) = 0 \quad (3.9)$$

$$m \frac{\partial f_0}{\partial \eta_j} - \kappa_{i,j} \left( \frac{d^2 \eta_j}{dx^2} \right) = 0 \quad (3.10)$$

And accordingly the integrated result

$$m f_0 - \frac{\kappa_{i,j}}{2} \left[ \left( \frac{d\eta_i}{dx} \right)^2 + \left( \frac{d\eta_j}{dx} \right)^2 \right] = 0 \quad (3.11)$$

Combination of equations 3.11 and 3.8 gives energy integral

$$\sigma_{i,j} = 2m \int_{-\infty}^{+\infty} f_0(\eta_i, \eta_j) dx \quad (3.12)$$

Change of integration variable from  $x$  to  $\eta_i$  gives

$$\sigma_{i,j} = \sqrt{2m\kappa_{i,j}} \int_0^1 \sqrt{f_0(\eta_i, \eta_j(\eta_i))} \sqrt{1 + \left( \frac{d\eta_j(\eta_i)}{d\eta_i} \right)^2} d\eta_i, \quad (3.13)$$

where function  $\eta_j(\eta_i)$  is the relation between order parameters along the interface. There is no analytical solution for this integral and that's why all the energy values should be calculated numerically for each and every case of individual set of model parameters  $\kappa$ ,  $\gamma$  and  $m$  because as will be seen further in this section the interfacial profile and function  $\eta_j(\eta_i)$  accordingly depend on all of these three parameters.

From Equations 3.9 and 3.10, it can be obtained

$$\frac{d\left(\frac{d\eta_j}{dx}\right)}{d\left(\frac{d\eta_i}{dx}\right)} = \frac{\eta_j^3 - \eta_j + 2\gamma_{i,j}\eta_i^2\eta_j}{\eta_i^3 - \eta_i + 2\gamma_{i,j}\eta_i\eta_j^2} \quad (3.14)$$

which tells that the right side of the relation depends only on one phenomenological parameter  $\gamma$ . Consequently,  $d\eta_j/d\eta_i$  and  $\eta_j(\eta_i)$  also depend only on  $\gamma$  parameter. Bringing together this conclusion and Equation 3.13, the following expression for the energy can be written

$$\sigma_{i,j} = g(\gamma_{i,j})\sqrt{\kappa_{i,j}m} \quad (3.15)$$

This expression shows how the model parameters contribute to the value of grain boundary energy which couldn't be investigated by the simplistic approach used in the Section 3.1.

### 3.2.1 Effect of model parameters on the interfacial profiles

Because the free-energy is symmetrical in terms of  $\eta_i$  and  $\eta_j$ , for symmetrical profiles there are these following relations:

$$\eta_j = 1 - \eta_i \quad (3.16)$$

$$\frac{d\eta_j}{dx} = -\frac{d\eta_i}{dx} \quad (3.17)$$

$$\frac{d^2\eta_j}{dx^2} = -\frac{d^2\eta_i}{dx^2} \quad (3.18)$$

Applying condition 3.18 to Equations 3.9 and 3.10 it comes that

$$\frac{\partial f_0}{\partial \eta_j} = -\frac{\partial f_0}{\partial \eta_i} \quad (3.19)$$

or taking derivatives according to the free energy having expression as in Equation 3.1

$$-(1 + 2\gamma_{i,j})\eta_i^3 + (3 + 2\gamma_{i,j})\eta_i^2 - 2\eta_i = -(1 + 2\gamma_{i,j})\eta_i^3 + 4\gamma_{i,j}\eta_i^2 - (2\gamma_{i,j} - 1)\eta_i \quad (3.20)$$

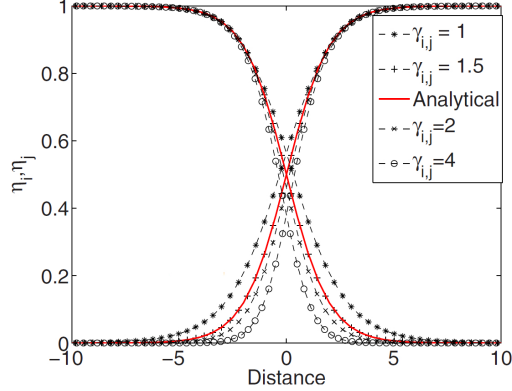


FIGURE 3.12: Numerically calculated interface profiles for  $\kappa=2.0$ ,  $m=1$  and different values of  $\gamma$ . From [37].

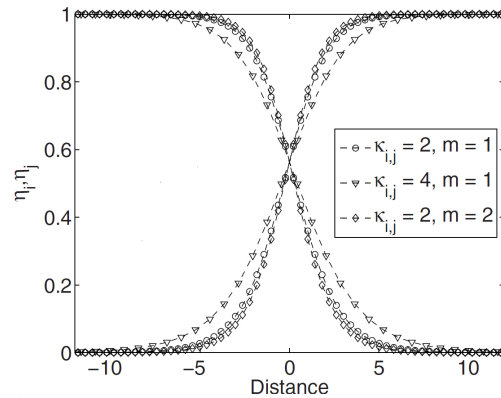


FIGURE 3.13: Numerically calculated interface profiles for  $\gamma=1$  and different  $\kappa$  and  $m$ . From [37].

This relation is true only for  $\gamma_{i,j}$  1.5.

For the symmetrical profiles of  $\eta_i, \eta_j$  the analytical solution of  $\eta_i, \eta_j$  can be derived,

$$\eta_i(x) = \frac{1}{2} \left[ 1 - \tanh \left( \sqrt{\frac{m}{2\kappa_{i,j}}} x \right) \right] \quad (3.21)$$

$$\eta_j(x) = \frac{1}{2} \left[ 1 + \tanh \left( \sqrt{\frac{m}{2\kappa_{i,j}}} x \right) \right] \quad (3.22)$$

For all other values of  $\gamma_{i,j}$  except 1.5, the interfacial profiles are not symmetrical. But there is no analytical solution for that. Numerical simulations are required to study the effect of phenomenological parameters  $\kappa$ ,  $\gamma$  and  $m$ . During these simulations the interfacial profiles start evolving from the flat surface and then come to the diffusive equilibrium shape. Results of the numerical simulation of phase field profiles for different values of  $\gamma$  and constant value of  $\kappa/m$  are shown in Figure 3.12 and for the same value of  $\gamma$  but different ratio of  $\kappa/m$  in Figure 3.13.

Because the free energy is symmetrical with respect to the phase field variables, the interfacial profiles have mirror symmetry with respect to the center of the grain boundary region. By analyzing these two figures it can be noticed that the value of profiles intersect,  $\eta_{interf}$ , depends on the parameter  $\gamma_{i,j}$  and does not depend on the parameters  $\kappa_{i,j}$  and  $m$ . And also Figure 3.12 proves the statement done before from mathematical calculations that symmetrical profiles appear only when the value of  $\gamma = 1.5$  is used.

### 3.2.2 Grain boundary energy

Looking back at Equation 3.8 it can be noticed that expression for the functional consists of two parts: a homogeneous contribution,  $mf_0$ , and a gradient part,

$$\frac{\kappa_{i,j}}{2} \left[ \left( \frac{d\eta_i}{dx} \right)^2 + \left( \frac{d\eta_j}{dx} \right)^2 \right].$$

According to the relation 3.11 it follows that both parts are equal along the grain boundary profile.

Considering  $\gamma = 1.5$ , analytical expressions can be derived for those two parts from Equations 3.21 and 3.22, which are the following:

$$mf_0(\eta_i(x), \eta_j(x)) = \frac{\kappa_{i,j}}{2} \left[ \left( \frac{d\eta_i}{dx} \right)^2 + \left( \frac{d\eta_j}{dx} \right)^2 \right] = \frac{m}{8} \left[ \cosh \left( \sqrt{\frac{m}{2\kappa_{i,j}}} x \right) \right]^{-4} \quad (3.23)$$

Maximum of both functions is reached at the center of the boundary region,  $x=0$ .

Again, for the interfacial profiles that are obtained for all other values except  $\gamma = 1.5$ , free-energy curves were calculated numerically and are shown in Figure 3.14 for different values of  $\gamma$  and constant  $\kappa$  and  $m$ , for the case of constant  $\gamma$  and different  $\kappa$  and  $m$  in Figure 3.15.

From Figure 3.14 it can be noticed that increase of  $\gamma$  follows with the increase of free-energy maximum at  $x=0$ . From Figure 3.15 it can be concluded that  $\kappa$  parameter has no effect on the height of the peak, but  $m$  does.

### 3.2.3 Anisotropic grain boundary properties

In the phase-field simulation length of the grain boundary plays a role of a parameter responsible for the stability and accuracy of the performed simulation [37]. That's why

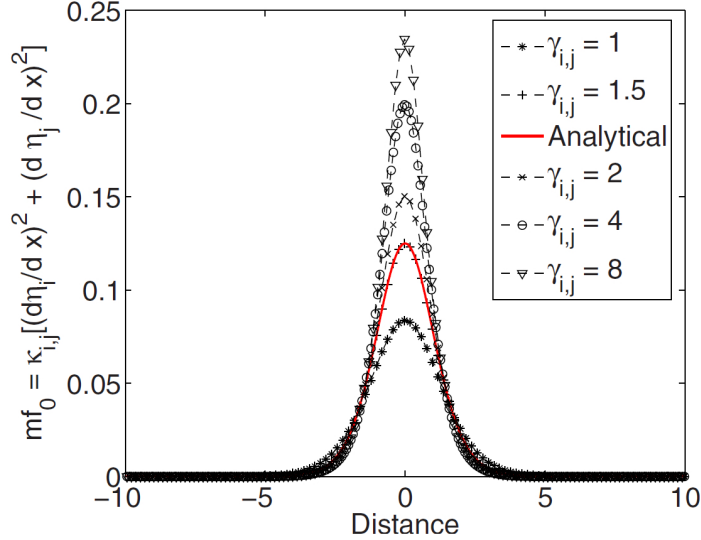


FIGURE 3.14: Homogeneous and gradient parts of the energy density across grain boundary region for  $\kappa=2.0$ ,  $m=1$  and different  $\gamma$ . From [37].

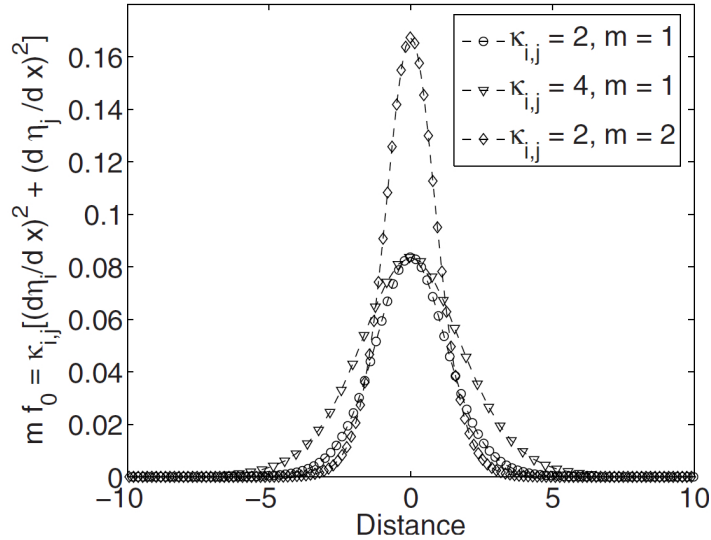


FIGURE 3.15: Homogeneous and gradient parts of the energy density across grain boundary region for  $\gamma=1$ , and different  $\kappa$  and  $m$ . From [37].

it is important how it is defined. The suggested way is based on the values of the phase field profiles at  $x=0$ :

$$l_{gb} = \frac{1}{|(d\eta_i/dx)_{x=0}|} = \frac{1}{|(d\eta_j/dx)_{x=0}|} = \sqrt{\frac{\kappa_{i,j}}{m f_{0,interf}}} \quad (3.24)$$

This definition can be used as sufficient for the stability and accuracy because the gradients get the maximum values at the center of the profiles. Analytical expression for grain boundary width for symmetrical profiles is

$$l_{gb} = \sqrt{\frac{8\kappa_{i,j}}{m}} \quad (3.25)$$

The expression for asymmetrical profiles can be obtained through numerical calculations of  $f_{0,interf}$ .

Combination together of relations 3.15, 3.24 and one known from the literature about phase-field

$$\mu_{gb}\sigma_{gb} = \kappa_{i,j}L_{i,j}, \quad (3.26)$$

gives the expressions for the model parameter which should reproduce the desired values of energy  $\sigma_{gb}$ , mobility  $\mu_{gb}$  and the thickness of the grain boundary which should be equal to  $l_{gb}$ . These are the following relations:

$$\kappa = \sigma_{gb}l_{gb} \frac{\sqrt{f_{0,interf}(\gamma)}}{g(\gamma)} \quad (3.27)$$

$$L = \frac{\mu_{gb}}{l_{gb}} \frac{g(\gamma)}{\sqrt{f_{0,interf}(\gamma)}} \quad (3.28)$$

$$m = \frac{\sigma_{gb}}{l_{gb}} \frac{1}{\sqrt{f_{0,interf}(\gamma)}} \quad (3.29)$$

### 3.2.4 Misorientation-dependent model parameters

All the above results are applied for the grain boundaries which have isotropic properties. But for the anisotropic case it should be extended so that parameters can reproduce misorientation-dependent behavior of grain boundary energy and mobility. The following procedure describes the way to get desired set of parameters when having a list of discrete values  $\sigma_{gb,k}$ ,  $\mu_{gb,k}$  and the width of boundary that should be achieved [37].

To be able to use the following algorithm, numerically calculated values of  $g(\gamma)$  and  $f_{0,interf}$  obtained from previous sections, should be fitted with some functions and used further for the calculation procedures. Before starting the main algorithm, arbitrary value of  $\gamma$  should be chosen ( $\gamma_{init}$ ). It is advised to choose this value around 1.5, so that interface profiles are close to symmetrical one. Then, use this value to calculate  $g(\gamma_{init})$ ,  $f_{0,interf}(\gamma_{init})$  and  $a_{init} = \sqrt{f_{0,interf}(\gamma_{init})}/g(\gamma_{init})$ . From the values of  $\sigma_{gb,init}$ ,

$f_{0,interf}(\gamma_{init})$ ,  $g(\gamma_{init})$  and  $l_{gb}$ , according to Equation 3.29,  $m$  parameter can be calculated. After this preliminary steps the main algorithm starts. New temporary variable  $a_k$  should be considered, which is

$$a_k = \sqrt{f_{0,interf}(\gamma_k)/g(\gamma_k)} \quad (3.30)$$

For every value of the grain boundary energy,  $\sigma_{gb,k}$ , and mobility,  $\mu_{gb,k}$ , the following steps should be performed:

1. From Equation 3.27 calculate  $\kappa^* = \sigma_{gb,k} l_{gb} a_{init}$
2. From Equation 3.15 calculate  $g(\gamma^*) = \sigma_{gb,k} / \sqrt{\kappa^* m}$
3. From the result calculated in Step 2 get the value  $\gamma^* = g^{-1}(\gamma)$
4. Get values of  $f_{0,interf}(\gamma^*)$  and  $a_k^*(\gamma^*)$
5. Compare  $a_k^*$  with  $a_{init}$ . If these values are equal, then  $\kappa_k = \kappa^*$ ,  $\gamma_k = \gamma^*$ ,  $a_k = a_k^*$  and  $L_k$  is calculated from Equation 3.28. If not, repeat the procedure with  $a_{init} = a_k^*$ .

After running this algorithm, lists of discretized phenomenological parameters  $\{\kappa_k\}$ ,  $\{\gamma_k\}$ ,  $\{L_k\}$  and  $m$  parameter are obtained, which allow to perform phase-field simulation of the anisotropic grain growth model.



# Chapter 4

## Results

### 4.1 Implementation of the algorithm for obtaining the misorientation-dependent model parameters

In Chapter 3 theoretical background and the algorithm are discussed, which allows for the given list of discretized grain boundary energies  $\sigma_{gb,k}$  and mobilities  $\mu_{gb,k}$ , where each single value correspond for a certain value of misorientation, to get the set of phenomenological parameters  $(\{\kappa_k, \gamma_k, L_k\}, m)$  which is needed eventually to solve Ginzburg-Landau equation.

As it was discussed before, many relations that allow the calculation of model parameters don't have analytical expressions and require the numerical calculation. This section is going to present the results of required numerical simulations and also the functions fitting the obtained points. These functions can easily be used for performing the model parameters calculation algorithm.

First step is to investigate how different values of  $\gamma$  affect the interfacial profiles of order parameters. A 1-dimensional two grain structure was built as model structure (shown in Figure 3.11).

Different values of  $\gamma$  parameter, from 0.1 to 20.00 with step of 0.05, were applied for normal grain growth simulation of such structure. In Figure 4.1 example of the interfacial profiles for some values of  $\gamma$  are presented.

The next goal was for the calculated results of grain boundary profiles to obtain values for the functions  $g(\gamma)$  and  $f_{0,interf}$ . Function  $f_{0,interf}$  was simply calculated by substituting the  $\eta_{interf}$  values, which are values of interface profiles intersection, into Equation 3.1. Figures 4.2 and 4.3 show the resulting points for the  $\eta_{interf}$  and  $f_{0,interf}$ , respectively.

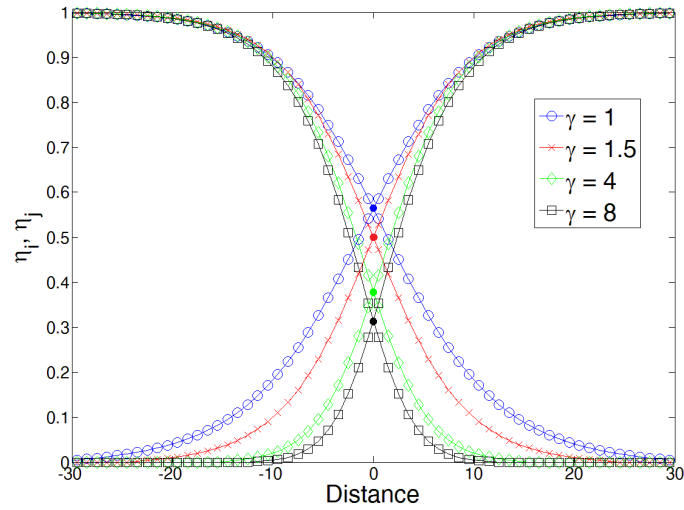


FIGURE 4.1: Numerically calculated profiles of two grain structure for  $\kappa = 2$ ,  $m=1$  and different values of  $\gamma$ . Solid points correspond to  $\eta_{interf}$  values, the intersection of the curves.

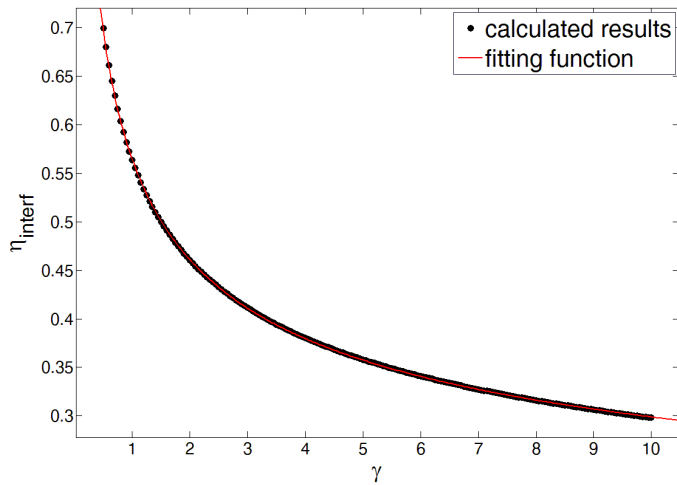
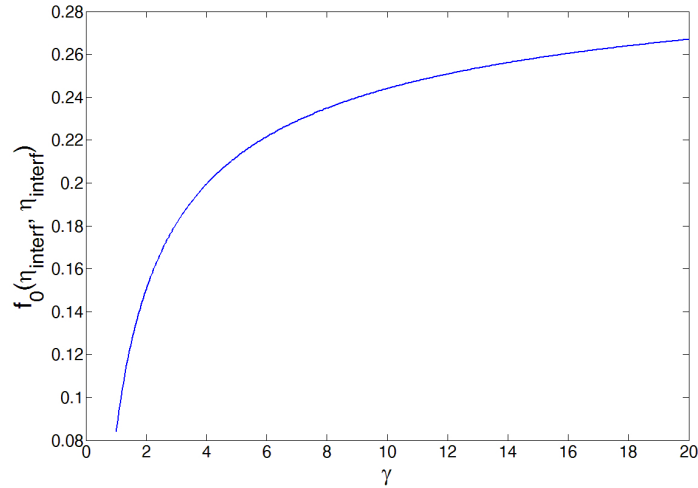
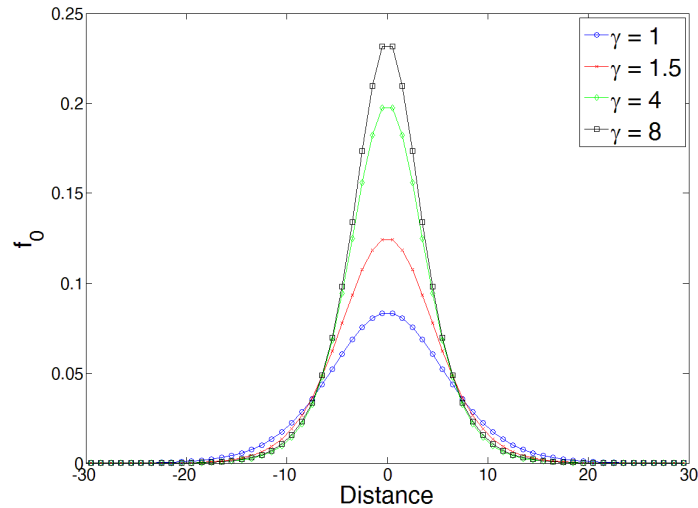


FIGURE 4.2:  $\eta_{interf}$  as a function of  $\gamma$  obtained from numerical studies.

For the ease of usage in the algorithm, points have been fitted with the following function

$$\eta_{interf}(\gamma) = 0.4764 * \gamma^{-0.3547} + 0.08842 \quad (4.1)$$

Function  $g(\gamma)$  can be calculated from Equation 3.15. Value of energy was integrated according to the Equation 3.12, where values of  $\eta_i$  and  $\eta_j$  were taken from the previously performed profiles calculation. In Figure 4.4 the free energy function plotted for different  $\gamma$  values is shown.

FIGURE 4.3:  $f_0(\eta_{\text{interf}}, \eta_{\text{interf}})$  as a function of  $\gamma$  obtained from numerical studies.FIGURE 4.4: Homogeneous energy density curve for different values of  $\gamma$ .

Resulting value for the  $g(\gamma)$  is obtained by dividing the grain boundary energy value over  $\sqrt{\kappa m}$ , where both parameters  $\kappa$  and  $m$  were keep constant and equal 2.0 and 1.0, respectively. In Figure 4.5 resulting calculated points are shown together with the fitting function.

As can be seen from the figure the calculated points can be fitted very well with the function

$$g(\gamma) = 0.7296 * (1 + 0.9793 * e^{-1.351\gamma}) - 0.524/\gamma. \quad (4.2)$$

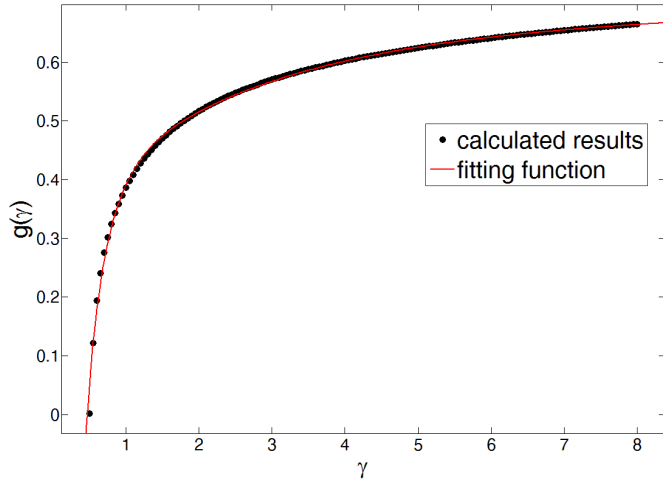


FIGURE 4.5: Numerically calculated function  $g(\gamma)$  connecting the grain boundary energy and  $\kappa, m$  parameters.

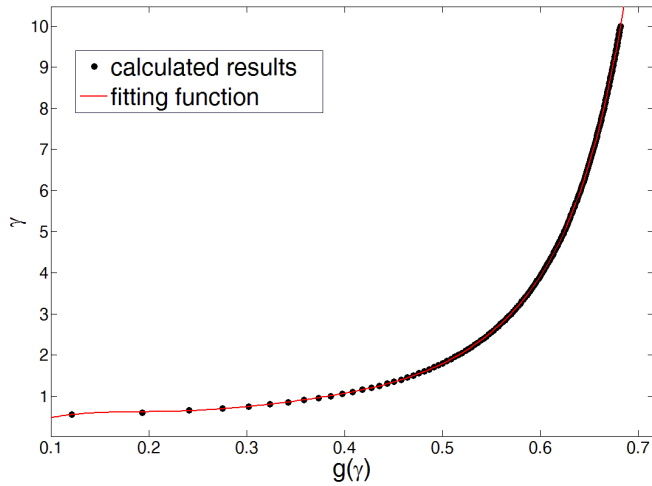


FIGURE 4.6: Inverse function for  $\gamma$  parameter, taking value of  $g$  as a parameter.

As long as values of  $\gamma > 0$ , results of this function outside of this range are not important. Algorithm procedure requires values of  $\gamma$  parameter as a function of  $g$ , namely the inverse value. Figure 4.6 shows the data points of such a function.

For this case it was also possible to get a function delivering sufficient fitting

$$\gamma = g^{-1}(g) = 35080 * g^8 - 95290 * g^7 + 108600 * g^6 - 66690 * g^5 + 23680 * g^4 - 4813 * g^3 + 515.3 * g^2 - 21.93 * g + 0.5267.$$

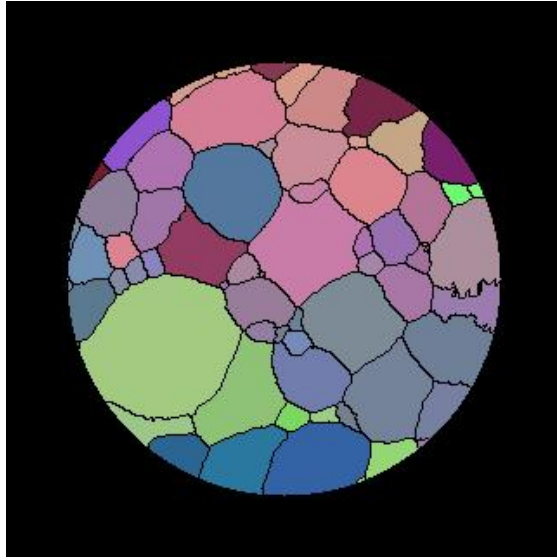


FIGURE 4.7: Two-dimensional slice 430 of the Al-1 wt.% Mg at the initial time step.

## 4.2 Two-dimensional anisotropic simulation results

Two-dimensional simulation, giving quite realistic and fast results, was chosen to begin with, rather than performing time consuming 3D simulation. This approach allows to get the first impression of the model which is used to reflect the possible microstructure evolution and study the effect of parameters variation which eventually might help during the 3D simulation for the purpose of getting the closest match with the experimental results.

The most intriguing part of the whole studying sample, Al-1 wt.% Mg, which was mentioned in the Introduction Chapter, is the slice 430, where one particular grain during the evolution gets much bigger in size comparing to the surrounding matrix. This slice at its initial step is presented in Figure 4.7 and was investigated with the help of two-dimensional phase field simulation.

More technical details have to be discussed. To make the phase field simulation working the set of phenomenological parameters should be chosen. As discussed in Section 3.2.4, the algorithm requires the list of the discretized values of grain boundary energy  $\sigma_{gb}$  and mobility  $\mu_{gb}$ . According to the anisotropic model, the energy and mobility for every grain boundary is dependent on the misorientation between the adjacent grains. Physically consistent relation for describing this misorientation-dependent behavior was derived by Read-Shockley and was discussed in Section 2.1.2.

This function is applied only for the low-angle grain boundaries. For the misorientations bigger than cutoff misorientation,  $\theta > \theta_m$ , the value of energy becomes constant and is equal to  $\sigma_m$ , which is a energy plateau. Different misorientation cutoff values were

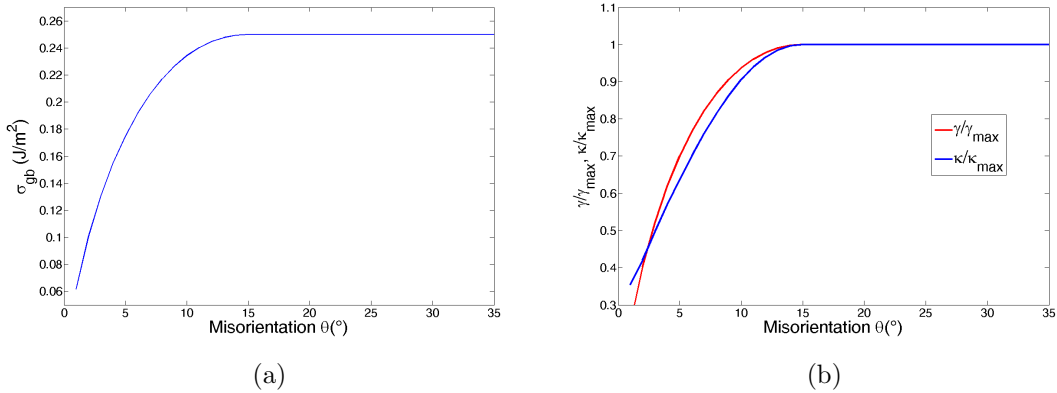


FIGURE 4.8: (a) Read-Shockley dependence of grain boundary energy as a function of misorientation and (b) calculated results of  $\kappa$  and  $\gamma$  parameters for these corresponding values of energies,  $\kappa_{max} = 0.25 \times 10^{-6} \text{ J/m}$ ,  $\gamma_{max} = 0.91$ .

studied and for every cutoff the Read-Shockley curve was obtained and discretized with the 0.01 precision. Obtained list of values was used as an input for the earlier discussed algorithm. According to the literature [40], value of  $\sigma_m$  was chosen to be  $0.25 \text{ J/m}^2$ , the grain boundary mobility was taken constant,  $\mu_{gb} = 1 \times 10^{-6} \text{ m}^2 \text{s/kg}$ , and the desired grain boundary width was taken  $l_{gb} = 1.33 \times 10^{-6} \text{ m}$ . Calculation of the phenomenological parameters as a part of algorithm gives  $m = 2.11 \times 10^6 \text{ J/m}^3$ ,  $L = 1 \text{ m} \cdot \text{s/kg}$ , values for  $\kappa$  and  $\gamma$  are presented in Figure 4.8.

Grid spacing discretization,  $dx$ , was equal to  $0.3 \times 10^{-6} \text{ m}$  ( $l_{gb} \approx 4dx$ ) and time step  $\Delta t = 0.01 \text{ s}$ . Resulting microstructure evolution at different time steps is shown on Figure 4.9.

It can be noticed that this grain of green color has higher growth rate and therefore its size is many times bigger than the grains around it. By looking at the Figure 4.10 such behavior can be explained with the fact that this grain is surrounded with high-angle grain boundaries, which tend to grow faster because they have higher energy.

The process of searching for the best match between the simulation results and experimental results lies in the change of parameters within allowed ranges until the microstructure with minimum difference with the experimental one can be obtained. One of the possible degrees of freedom for the parameter variation in the anisotropic systems is the variation of cutoff misorientation. As was previously discussed in the Theory part, maximum value of the misorientation that can appear in the system is  $62.8^\circ$  and according to the misorientation distribution that is unique to the sample, with a certain probability every misorientation can appear in the microstructure. Change of cutoff misorientation allows some grains to grow faster than others and depending on the misorientation distribution can affect the microstructure evolution in a different ways. As can be seen from Figure 4.11, significant amount of grains are low-angle boundaries and

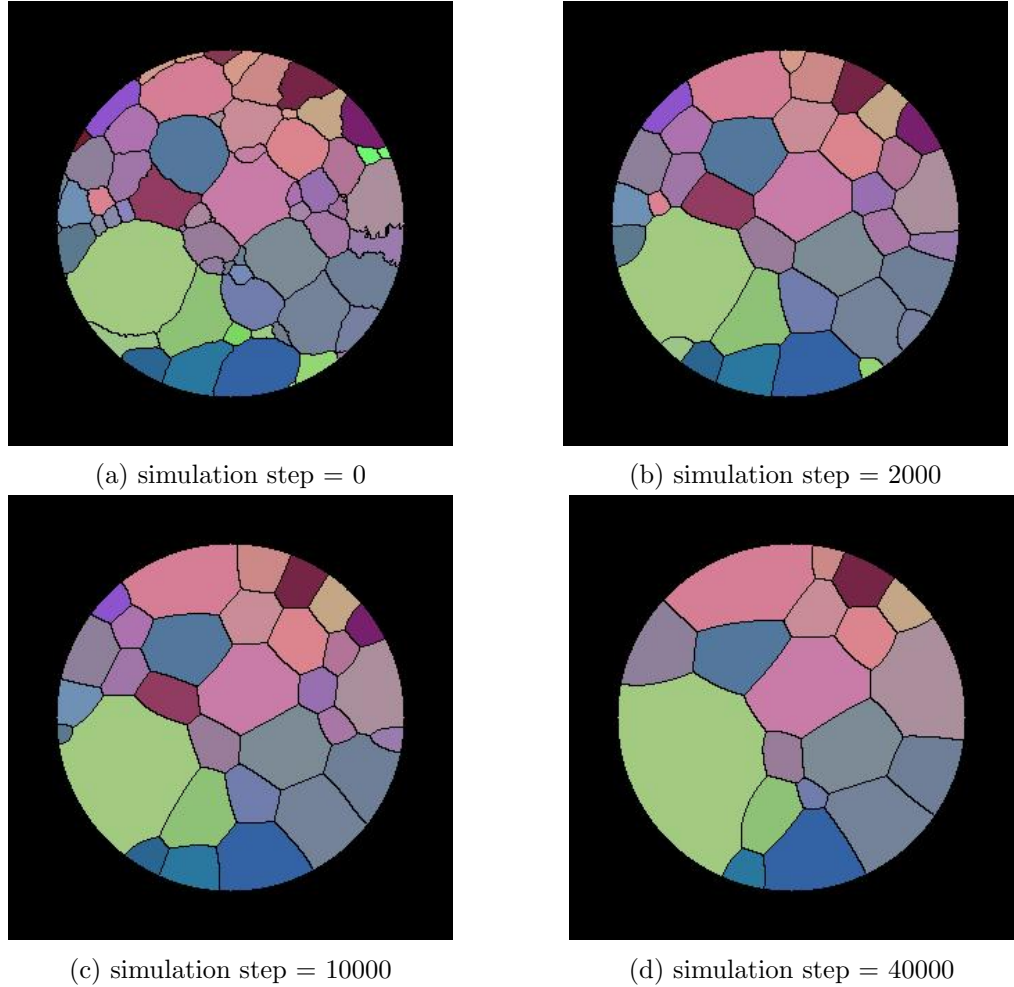


FIGURE 4.9: Two-dimensional phase field simulation results of the anisotropic growth with the cutoff misorientation  $\theta_m = 15^\circ$  and Read-Shockley relation between the grain boundary energy and misorientation.

according to this change of cutoff misorientation can bring noticeable deviation in the microstructure evolution.

Figure 4.12 demonstrates how different cutoff misorientation affects the resulting microstructure. Apparently, the effect from variation of cutoff misorientation, at least for  $\theta_m \leq 15^\circ$ , doesn't change sufficiently the resulting microstructure, except for some small grains.

Two-dimensional simulation gave some rough idea of how the grain evolution proceeds, but sometimes effect from real three-dimensional size of the grains and their interconnectivity might have significant effect on the resulting microstructure. Therefore, it was decided to continue only with three-dimensional simulations, results to which are discussed in the next section.

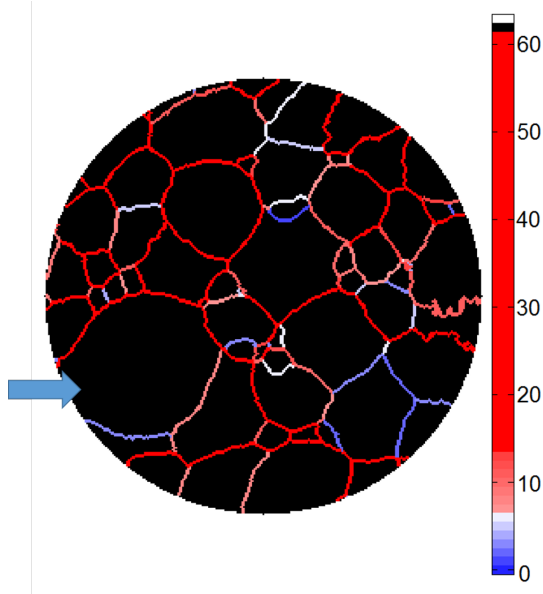


FIGURE 4.10: Colored scheme of the grain boundaries. Red grain boundaries are high-angle grain boundaries with high energy and blue grain boundaries are low-angle grain boundaries with low boundary energy. Presence of the high-angle grain boundaries around the grain marked with arrow allow it to obtain bigger growth rate in the upwards direction.

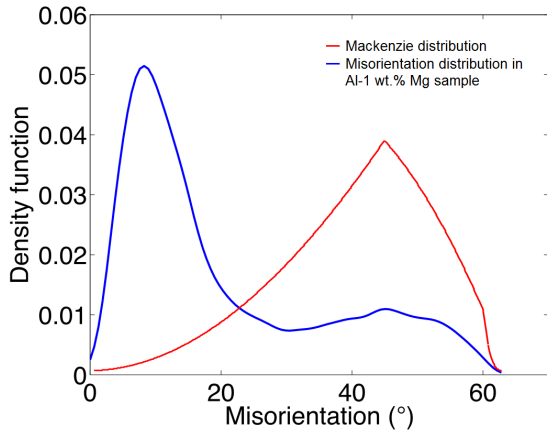


FIGURE 4.11: Misorientation distribution of the studied Al-1 wt.% Mg. Shape of the curve differs greatly from the Mackenzie distribution. Most of the grain boundaries are low-angle.

### 4.3 Three-dimensional anisotropic simulation results

The whole sample which is investigated in this thesis work was shown previously in the Introduction part in Figure 1.1. The desired slice of simulation which contains a grain, the one that was desired to investigate abnormal grain growth, is located close to the top surface of the sample. Taking into considerations that simulating the whole structure of the whole sample even on the modern computer takes almost a week, upper half of the sample, which is able to cover the abnormal grain, mentioned in the previous section,

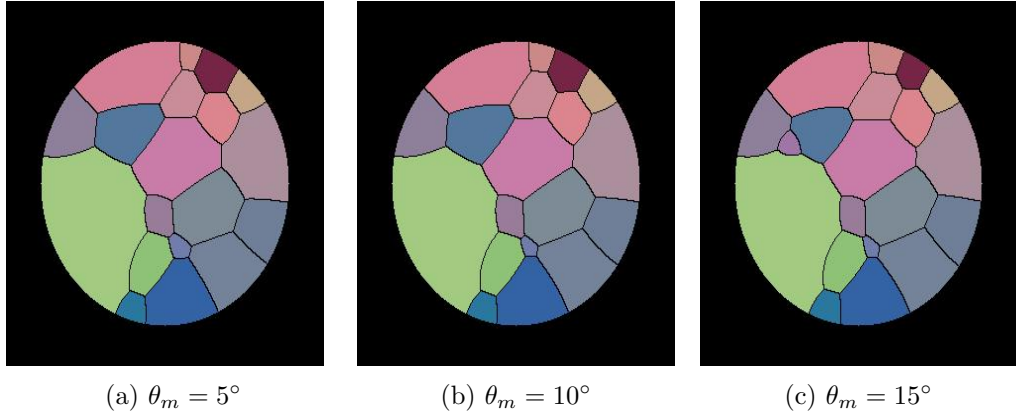


FIGURE 4.12: Comparison of the anisotropic simulation for different values of cutoff misorientation after equal amount of simulation steps(40000). Change of cutoff misorientation  $\theta_m$  does not have significant influence on the sizes of the grains and the grains morphology for  $\theta_m \leq 15^\circ$ .

and its neighbors, was used for simulation and was analyzed in this section and following chapter.

As was discussed in the previous section related to the simulation of the two-dimensional microstructure, variation of the cutoff misorientation is one possible parameter that can be changed. When speaking about anisotropic grain growth, anisotropic energy, anisotropic mobility or its combination might be considered. It was decided to study these parameters individually and in combination with each other.

For the following 3D results it should be noted that parameters like grain boundary width,  $l_{gb}$  and  $m$  were keeping the same. Unless it is pointed that the grain boundary energy or mobility has a certain constant value, Read-Shockley relation is assumed.

### 4.3.1 Anisotropic Energy and Constant Mobility

Three-dimensional simulation was done for the case of anisotropic energy with  $\sigma_m = 0.25J/m^2$  and constant mobility equal to  $1 \times 10^{-6}m^2s/kg$ . Figure 4.13 gives an example of simulation microstructure in 3D.

In Figure 4.14 results for the three-dimensional simulation are presented showing two-dimensional slice at different time steps. Looking back to the results presented for the two-dimensional simulation, the difference in the microstructure evolution can be noticed (Figure 4.15).

Different cutoff misorientations were investigated, in particular  $\theta_m = 5^\circ, 10^\circ, 15^\circ$ . Results for this investigation are shown in Figure 4.16. By comparing with experimental results (Figure 4.16 (a)), conclusion can be drawn that simulation with  $\theta_m = 15^\circ$  brings

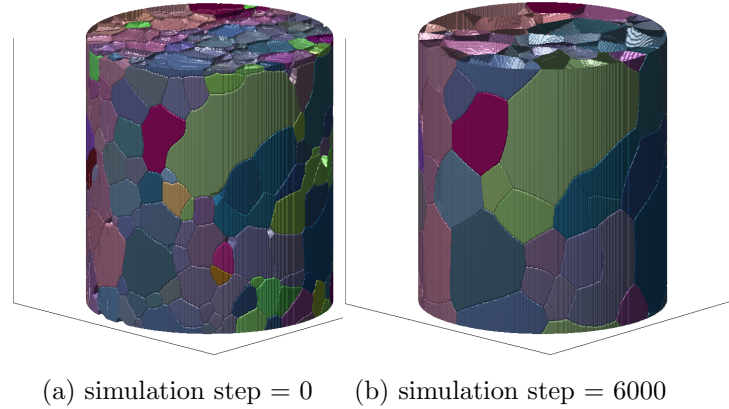


FIGURE 4.13: Three-dimensional representation of the simulation results. Anisotropic energy, constant mobility, cutoff misorientation  $\theta_m = 15^\circ$  were used.

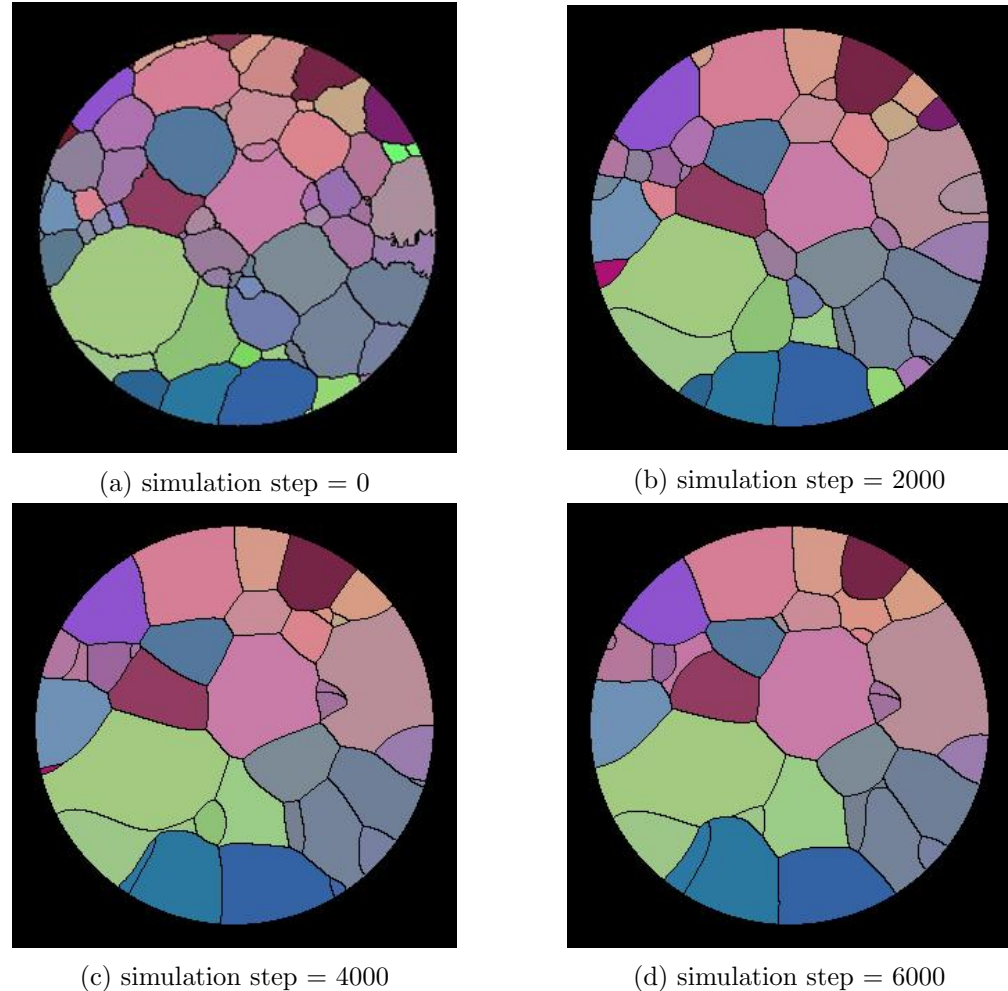


FIGURE 4.14: 3D simulation under consideration of anisotropic energy and constant mobility. Time evolution of the studying sample shown as two-dimensional slice with provided amount of simulation steps performed.

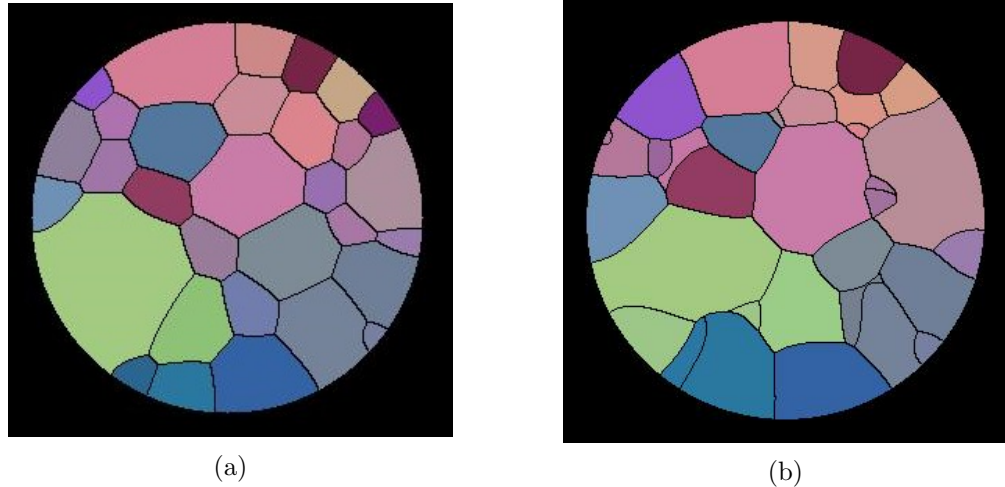


FIGURE 4.15: Slice simulated in 2D (a) and 3D (b) (shown at the same slice for 2D simulation). Starting from same microstructure are shown at the time step 6000. Observed difference between resulting microstructures comes from the effect of topology.

a closer match than other two cutoff misorientations. This can be seen from the comparison of the big green grain between all three simulations. With increase of the cutoff misorientations, the size of this grain is increasing and at the same time the matrix is not significantly affected.

### 4.3.2 Anisotropic Mobility and Constant Energy

In this section mobility was assigned to be anisotropic with the value at plateau equal to  $1 \times 10^{-6} \text{ m}^2/\text{s}/\text{kg}$  and the energy is constant for all grain boundaries,  $\sigma = 0.25 \text{ J/m}^2$ .

In Figure 4.17 simulation results are shown, from which it can be concluded that even within sufficient amount of simulation steps a certain grain shown with an arrow, doesn't shrink but slowly increases its size when the mobility is anisotropic and energy is constant. Presence of this grain in the simulation contradicts with the experimental results. Figure 4.18 shows that cutoff misorientation does not affect the grains morphology. Comparing this with any of previous results for the case of anisotropic energy tells that use of anisotropic mobility does not provide better results in terms of fitting with experimental results.

### 4.3.3 Anisotropic Energy and Anisotropic Mobility

As it was seen from two previous sections, incorporation of the anisotropic behavior of the grain boundary energy and mobility individually leads to the different resulting microstructure. Therefore, combination of both was also studied. As the previous

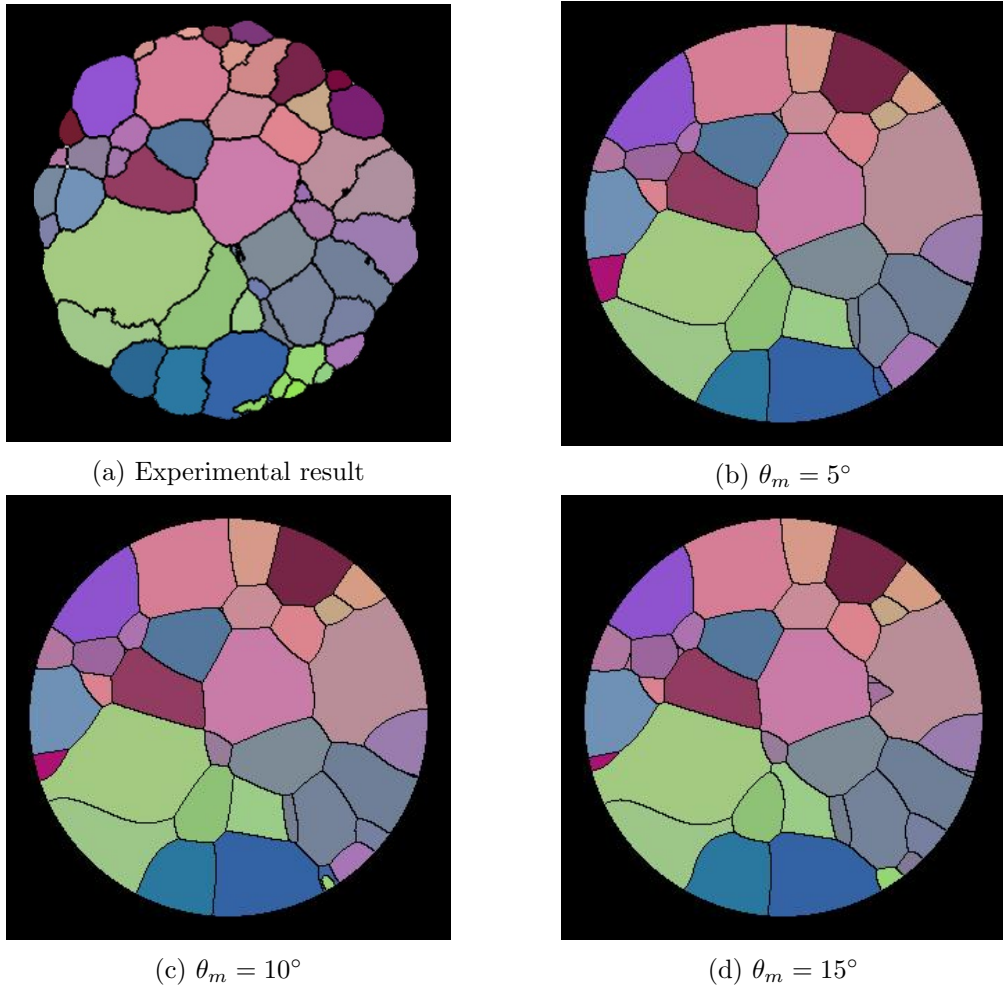


FIGURE 4.16: Experimental and simulation microstructures (3000 simulation steps) shown here were chosen in the matter of minimum difference. Further comparison proves qualitatively that simulation done with cutoff misorientation  $\theta_m = 15^\circ$  predicts result closer to experimental ones than when the lower values of cutoff misorientation is used, because the size of the big green grain is the biggest in simulation with cutoff  $15^\circ$  while the matrix grains are similar in size and morphology within all three cutoff misorientations.

results are showing, despite the fact that reasonable amount of grains have low-angle grain boundaries, change of the misorientation cutoff does not bring the interested grain to dramatic growth rate which will result in abnormal growth, which is observed in the experiment (Figure 4.19). That's why in this section abnormal grain growth was studied involving anisotropic energy and mobility with the conventional cutoff misorientation  $\theta_m = 15^\circ$ .

In Figure 4.20 the time evolution is shown together with three-dimensional representation of the grains marked with arrows. The one of green color is the grain that grows abnormally in the experiment but in simulation grows very slowly. It can be noted qualitatively that the red and blue grains neighboring with the green one within reasonable amount of simulation steps don't change its volume. And for that reason they are

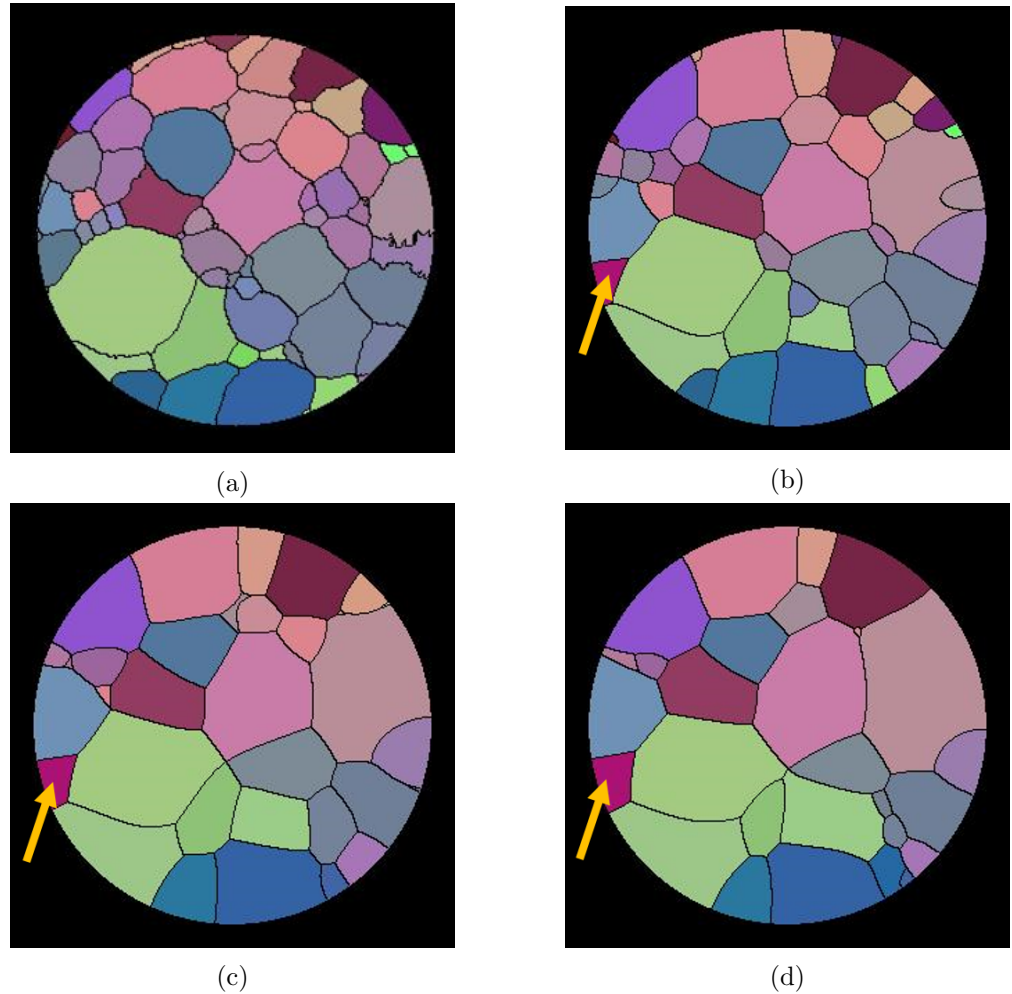


FIGURE 4.17: A 2D cross-section of 3D dataset simulation for the case of grain boundaries having anisotropic mobilities and the cutoff misorientation  $\theta_m = 15^\circ$ . Simulation time steps 0, 2000, 4000 and 6000 correspond to a,b,c,d, respectively. Grain marked with arrow does not appear in the experiment.

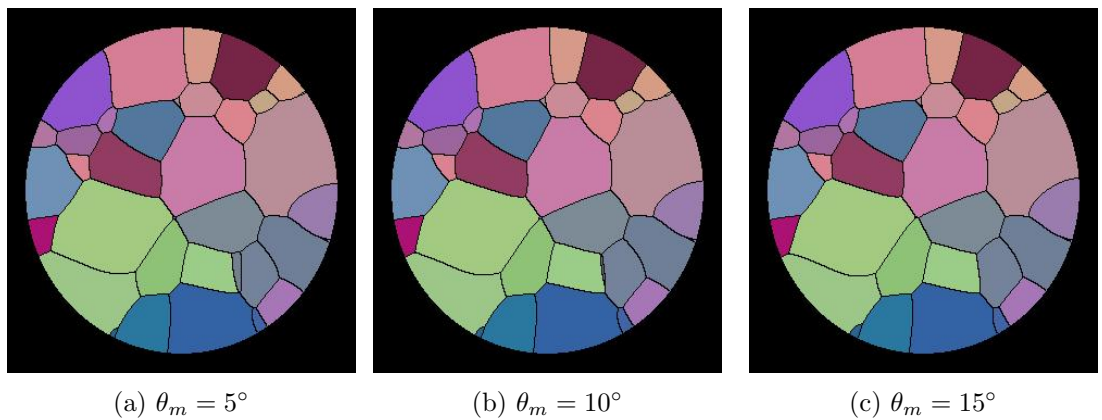


FIGURE 4.18: Change of cutoff misorientation almost does not affect the resulting microstructure.

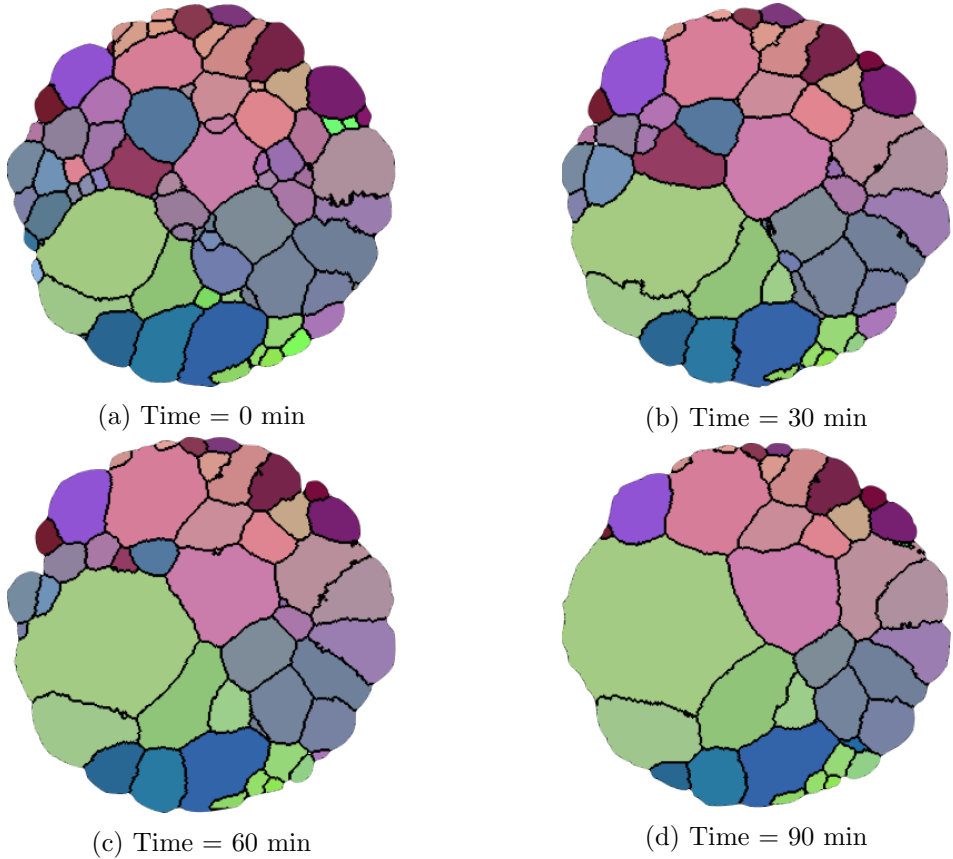


FIGURE 4.19: Cross section of the slice 430 from the experimental sample at different annealing time steps.

preventing the green grain to grow in that direction.

But by comparing between these results with the ones coming from the model involving only anisotropic energy it can be seen from Figure 4.21 that simulation with both anisotropic energy and mobility in the region downward from the big green grain matches better with experiment than the simulation with only anisotropic energy, while the rest of microstructure between two models don't differ so much. Possible ways to improve matching between the simulation and experiment along with some quantitative comparative analysis between normal and abnormal grain growth simulation and experiment is discussed in the next chapter.

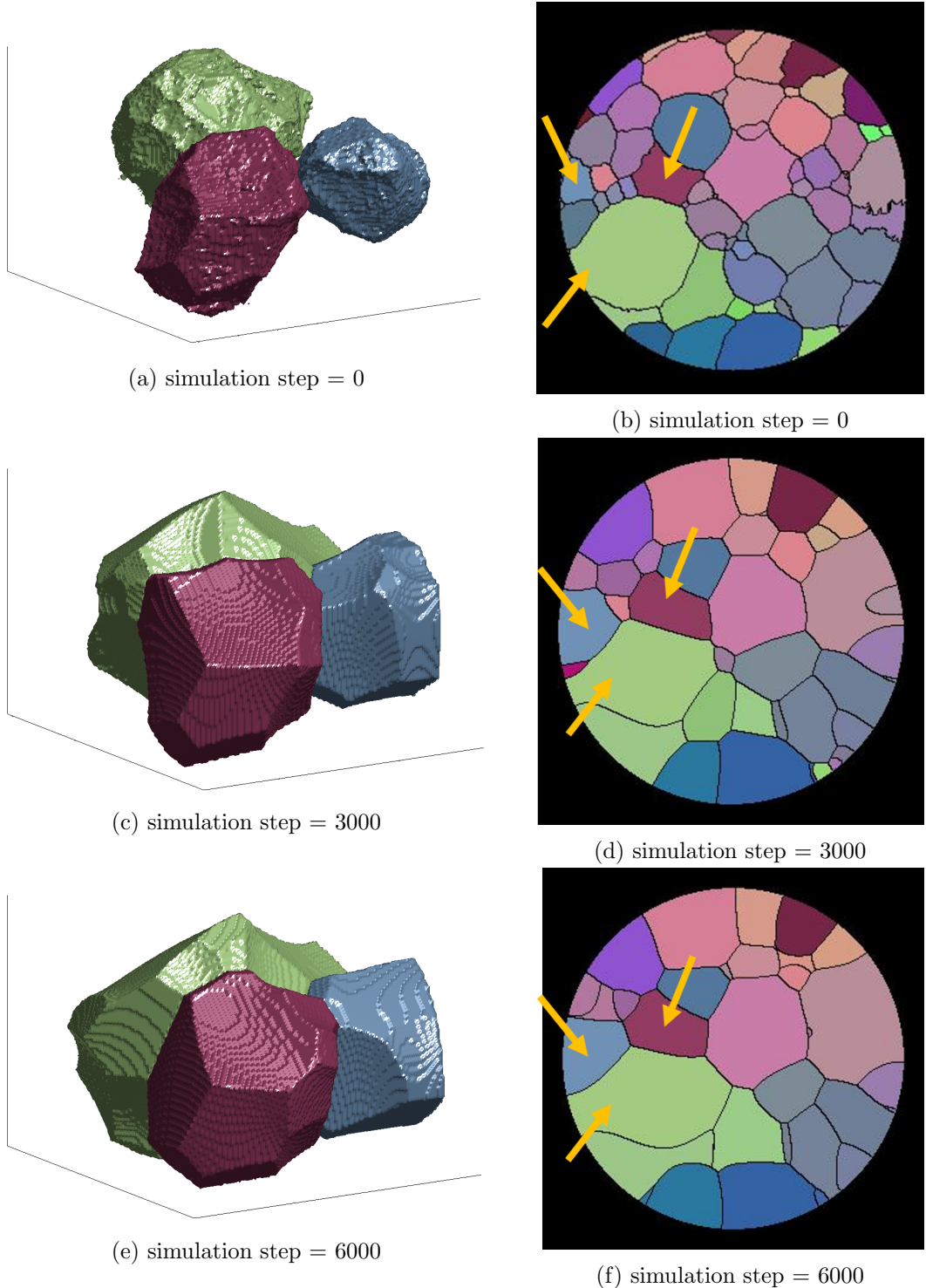


FIGURE 4.20: Three-dimensional volume investigation of the green grain that is supposed to grow abnormally. Surrounded grains shown with the red and blue color are not changing their volume within long time therefore blocking the green grain from abnormal grain growth. (b), (d), (f) are cross-section results from three-dimensional phase field simulation with the boundaries having both anisotropic energies and mobilities.

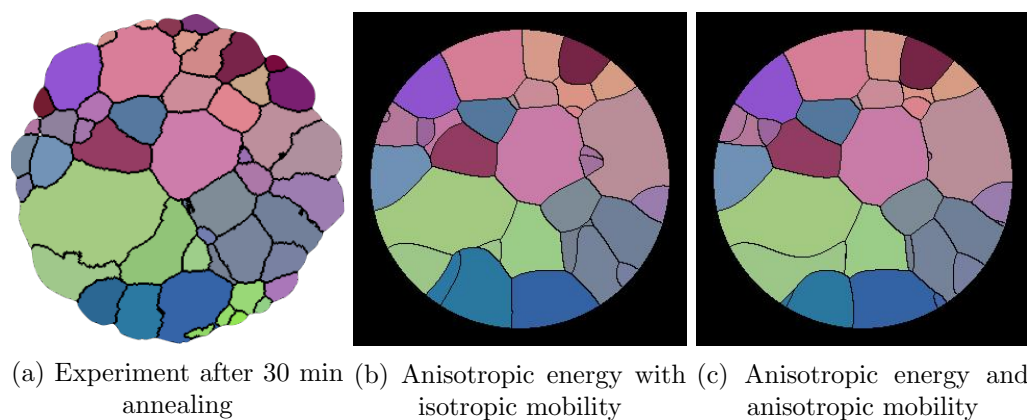


FIGURE 4.21: Comparison between different anisotropic models. The one which involves both anisotropic energy and mobility gives closer match with experiment than the model where only energy is anisotropic.

# Chapter 5

## Discussion

### 5.1 Qualitative Analysis

In the Results Chapter different parameter configuration was investigated in terms of cutoff misorientation, application of anisotropic paradigm individually to energy, mobility and its combination. From all these results, situation with anisotropic energy and mobility and cutoff misorientation equal to  $\theta_m = 15^\circ$  has shown closest match to experimental results when compared with energy or mobility alone being anisotropic. Since comparison of the whole 3D volume is complicated, one possible approach I take in this thesis is to concentrate on the grains which grow abnormally (Figure 4.19). The simple goal that should be achieved is to repeat the behavior of that grain having abnormal growth within the annealing time. In simulation (Figure 4.20) abnormal growth of the desired grain is suppressed by the neighboring grains being of the same size for a long simulation time. In this section attempts to solve this problem qualitatively would be discussed followed by more quantitative comparison in the next section.

#### 5.1.1 Shifting cutoff misorientation to higher values

In Sections 4.3.1, 4.3.2, 4.3.3, the idea to decrease the cutoff misorientation angle was inspired by the fact that in experimental data, significant amount of grains have small misorientation values ( $< 20^\circ$ ) (Figure 4.11). This means that only few grain boundaries would have high energy if the misorientation  $\theta_m = 15^\circ$  is applied. Therefore, involving more grain boundaries to higher rate evolution is supposed to give noticeable effect on the microstructure. As shown in previous chapter, this approach does not give better match with experiment.

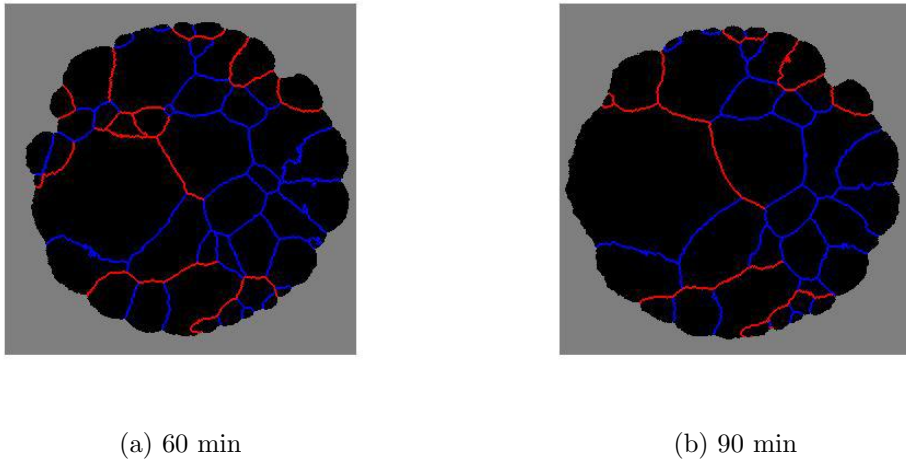


FIGURE 5.1: Experimental results of the microstructure from slice 430 after 60 min (a) and 90 min (b) annealing. Colorized boundaries represent high (red) and low (blue) angle grain boundaries. If we can set cutoff misorientation to  $\theta_m = 32^\circ$  then it was proposed to get the abnormal growth.

New idea was taken by studying the possible reasons of sudden extreme size increase happened between 60 min and 90 min of annealing time for experimental data (Figure 4.19). It was intended to assign such a cutoff misorientation value that allows having sufficient amount of high angle grain boundaries in the upper half of anisotropic grain, in order to let it grow abnormally, and the rest matrix of grains with as much low angle grain boundaries as possible in order to slow down the growth of the surrounding matrix. Figure 5.1 clarifies the eventual choice for cutoff misorientation equal to  $32^\circ$ .

Results shown in Figure 5.2 prove the ability of desired grain to grow bigger in size and the two suppressing grains to shrink. Systematic study of even further increase of cutoff misorientation followed with the unpredictable grains appearing from lower slices of the three-dimensional microstructure and suppressing the further growth of the desired grain. Therefore, the conclusion was done that cutoff misorientation should be assigned close to value of  $\theta_m = 32^\circ$ .

Comparing with previously studied cutoff misorientation  $\theta_m = 15^\circ$ , as shown in Figure 5.3, it can be concluded that cutoff misorientation  $\theta_m = 32^\circ$  gives significantly better results in terms of grains morphology. This difference can be explained with the fact that more high-angle grain boundaries are involved into the evolution process when the cutoff misorientation  $\theta_m = 15^\circ$  is used, that's why more grains are moving faster.

From Figure 5.2 it can be seen that it was able to achieve the desired grain to grow, however, in experiment, while this green grain grows abnormally, the rest of the grains were having still relatively smaller size, which is not observed for these simulation results. Different approaches are going to be discussed to achieve this kind of growth.

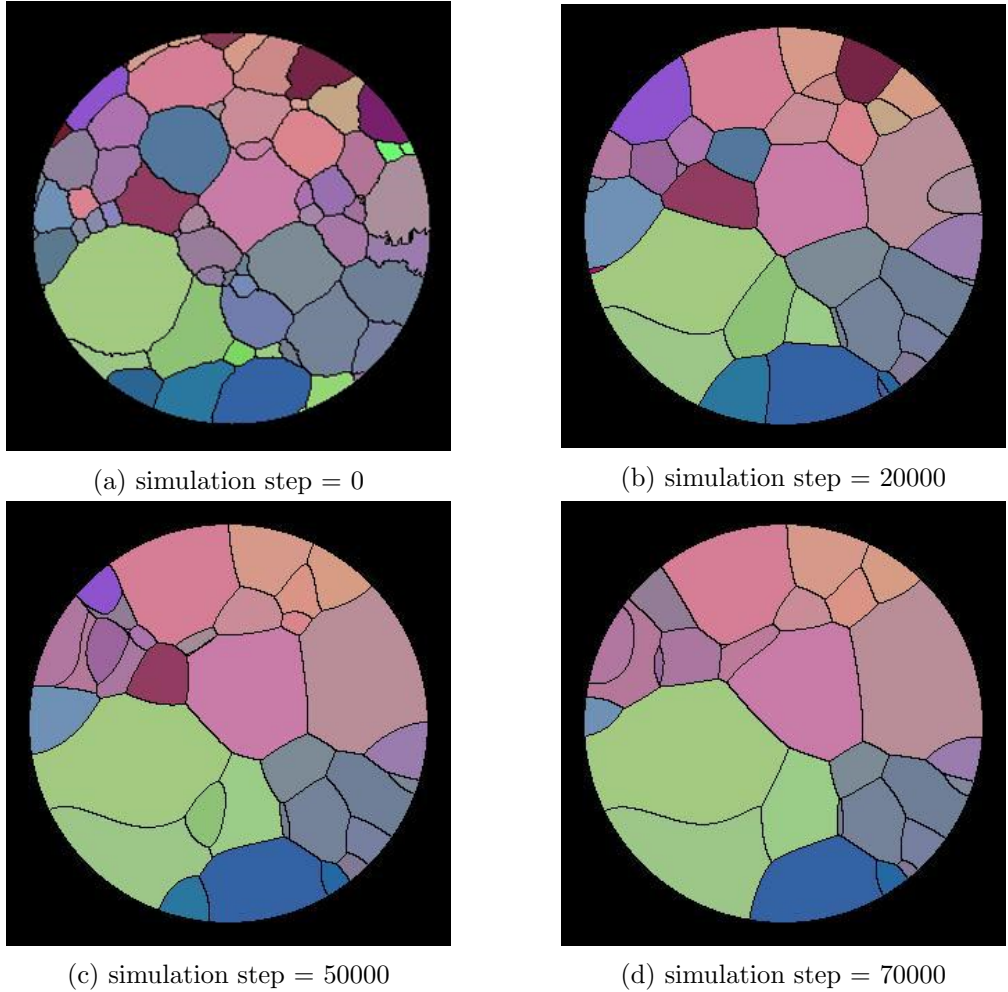


FIGURE 5.2: Anisotropic 3D simulation presented as slice 430 at different simulation steps. Both the grain boundary energy and mobility are anisotropic and the cutoff misorientation is  $\theta_m = 32^\circ$ . Green grain is growing bigger, however, matrix grains are bigger in size compared to experimental data.

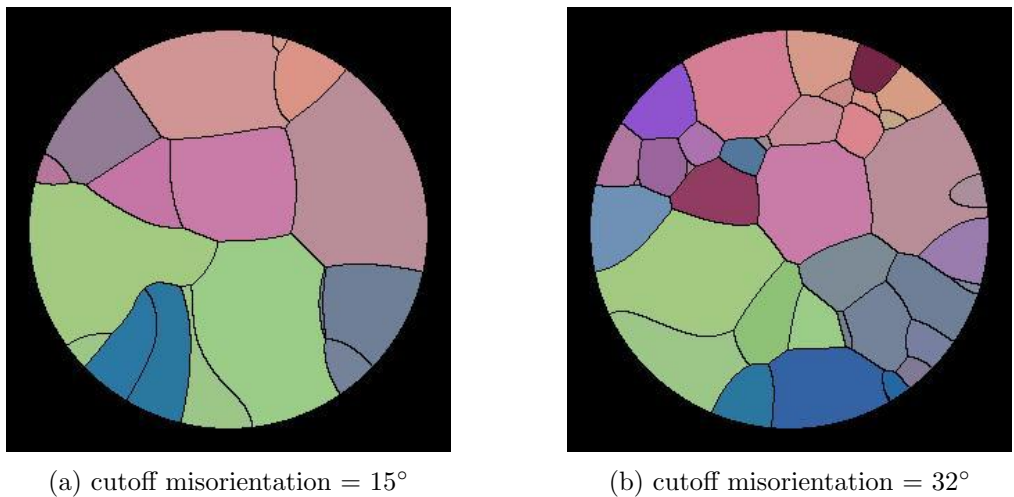


FIGURE 5.3: Microstructure comparison after 30000 simulation steps for different cutoff misorientation used.

### 5.1.2 Experimenting with different values of energy plateau

Intention to increase the growth rate of the desired grain theoretically can be done with the increase of plateau energy,  $\sigma_m$ . As long as that grain is surrounded with the high angle grain boundaries, increased energy plateau means higher velocity and therefore leading to abnormal growth. But in 3D simulation great role is also played by the topology factor of growth. Because of complicated spatial volume distribution, it is hard to predict influence from neighboring grains at different slices of the microstructure. Therefore the following investigation is considered as qualitative analysis.

In Figures 5.4 (a), (c), (e) and 5.4 (b), (d), (f) energy plateau,  $\sigma_m$ , was assigned to different values, equal  $0.5 \text{ J/m}^2$  and  $1.0 \text{ J/m}^2$  respectively. Increase of plateau energy is followed with grains from lower slices to affect the microstructure evolution. Till some point the biggest grain of the green color is increasing in size with the following decrease due to the size dominance of neighboring grains.

### 5.1.3 Contribution from the anisotropic mobility

From literature overview many researchers claim that anisotropic mobility alone almost does not affect the microstructure evolution [41, 42]. But mostly those investigations were done for two-dimensional simulation, which don't consider topology effects from real three-dimensional space. In order to investigate this, simulation was done with all the boundaries having the same value of energy equal to  $\sigma = 0.25 \text{ J/m}^2$  and the mobility depending on the misorientation according to the Read-Shockley relation. Resulting microstructure evolution and comparison with the results of NGG are shown in Figure 5.5.

It can be noticed that very small difference exist between these two types of growth. According to this, conclusion can be drawn that the anisotropic mobility along with isotropic energy almost does not affect the microstructure evolution.

According to this conclusion, results obtained in the previous Section 5.1.1 can be achieved also by involving only anisotropic energy and keeping the mobility constant for all grain boundaries. In order to investigate how anisotropic mobility influences the microstructure evolution when the grain boundaries have anisotropic energies, in the simulation done in Section 5.1.1, anisotropic mobility was replaced with the constant value equal to the value of plateau  $1.0 \times 10^{-6} \text{ m}^2/\text{s/kg}$  (Figure 5.6).

In the Figure 5.6 it can be seen that the grain marked with the yellow arrow is growing faster than in the experiment leading it to the contact with the big grain of the green

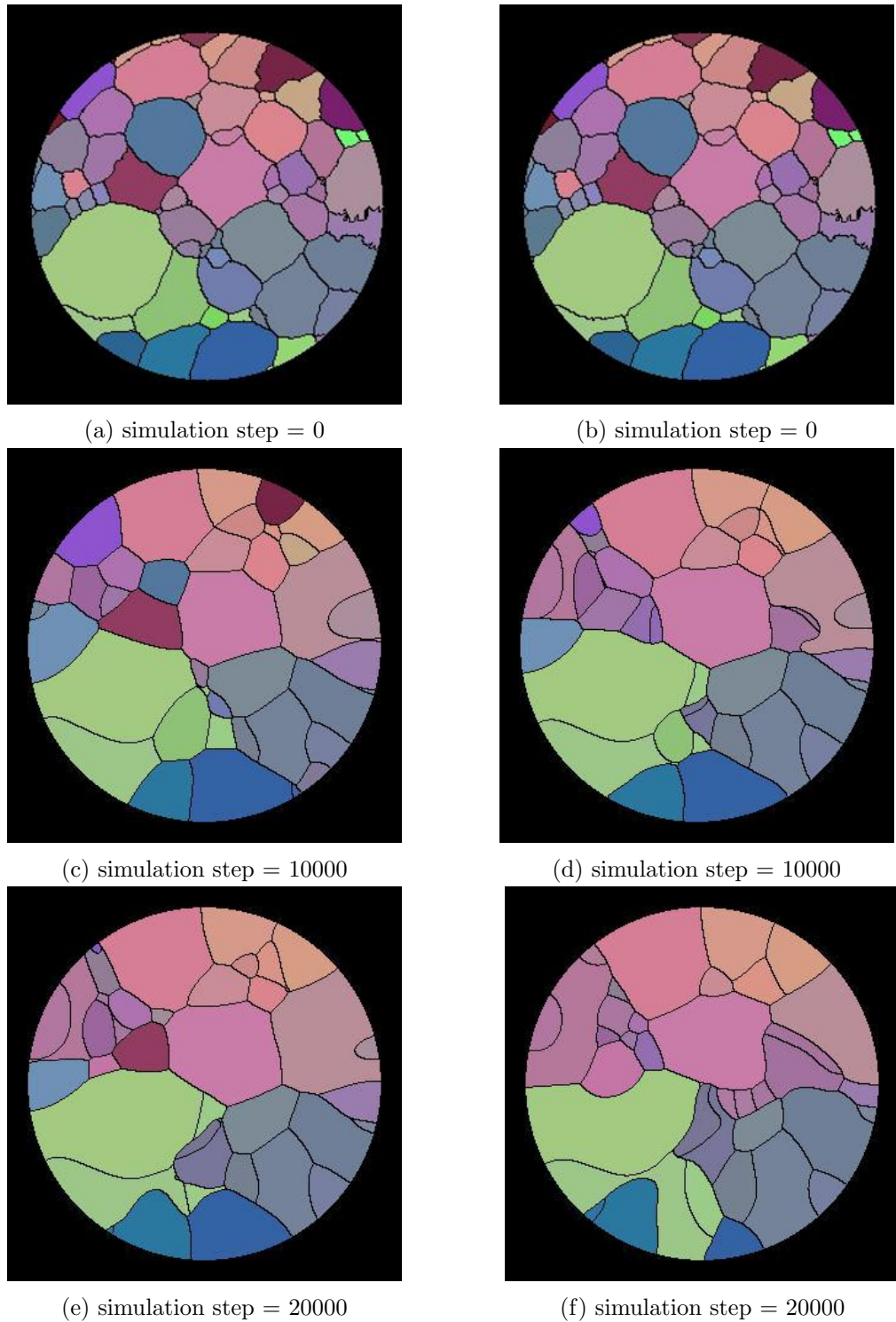


FIGURE 5.4: Anisotropic model with both anisotropic energy and mobility. Plateau value of energy for (a), (c), (e) is equal to  $0.5 \text{ J/m}^2$ . Plateau value of energy for (b), (d), (f) is equal to  $1.0 \text{ J/m}^2$ . Increase of energy plateau higher than  $0.25 \text{ J/m}^2$  results in a worse match with experiment.

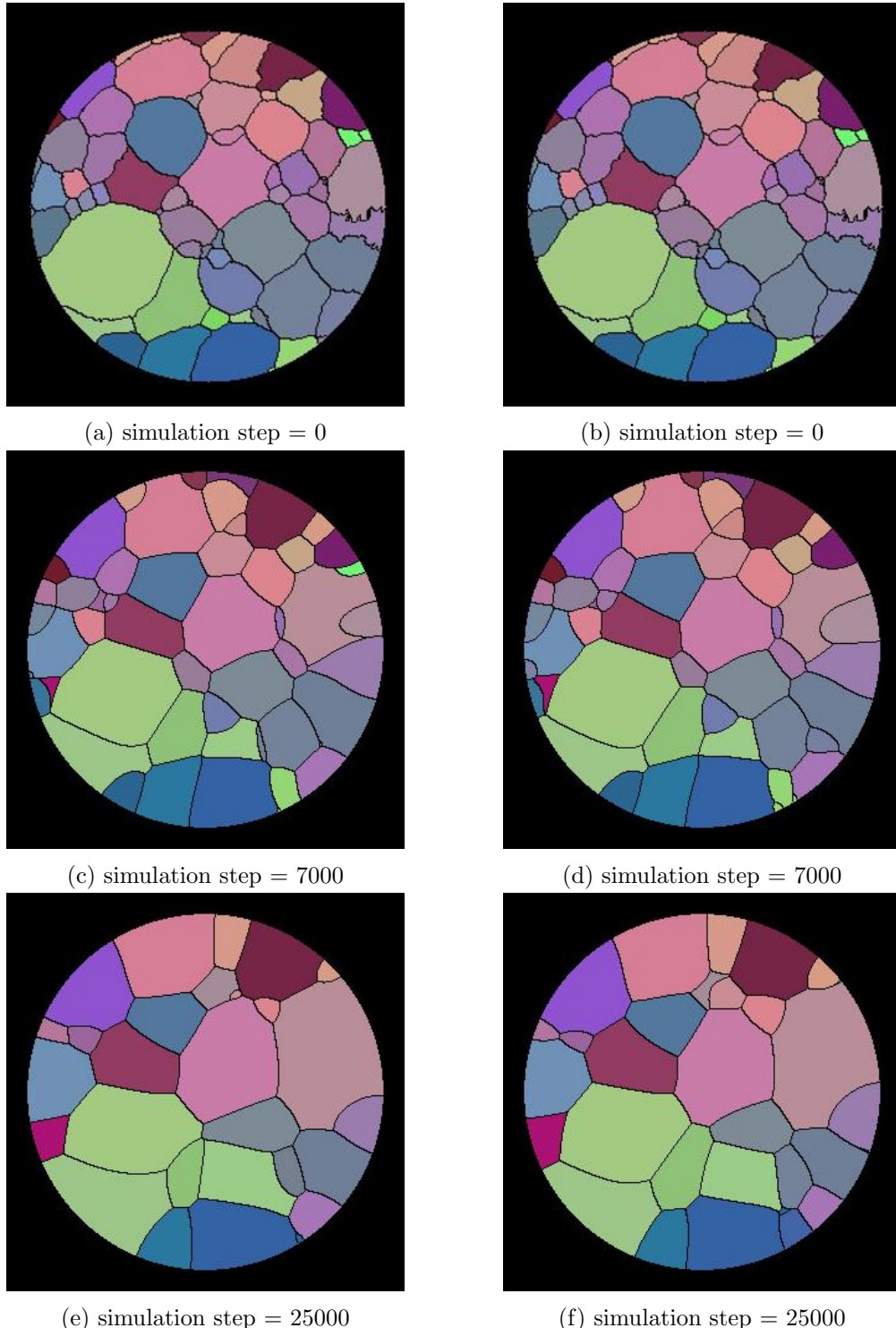


FIGURE 5.5: Comparison between the NGG (a), (c), (e) and AGG simulation (b), (d), (f) with anisotropic mobility and constant value of energy, cutoff misorientation  $\theta_m = 32^\circ$ . Anisotropic mobility model gives similar results as NGG simulation.

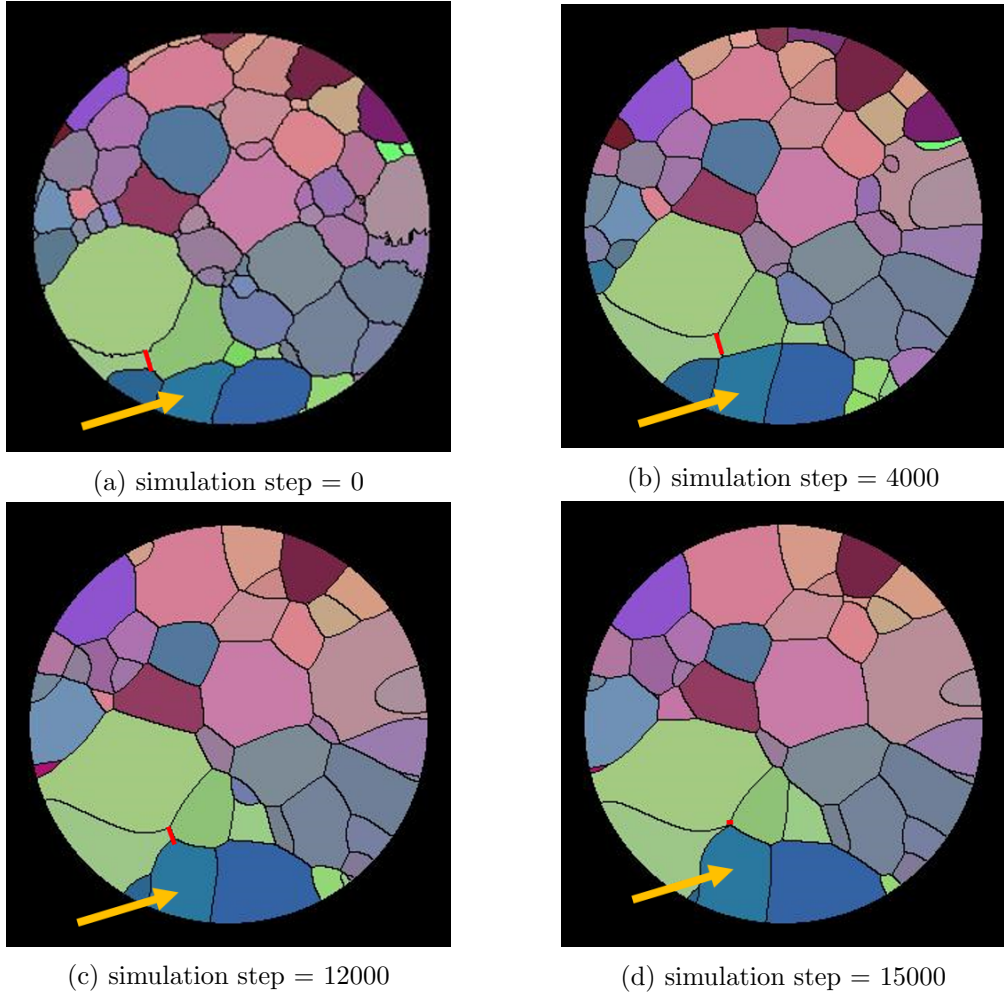


FIGURE 5.6: Simulation results with anisotropic energy and constant value of mobility. Cutoff misorientation for grain boundary energy is  $\theta_m = 32^\circ$ . Grain marked with yellow arrow during evolution comes into contact with the big green grain through shrinking of the grain boundary of the red color, which contradicts with experimental results. Results in the previous Section 5.1.1 show that incorporation of anisotropic mobility into simulation does not allow the grain, marked with yellow arrow, to grow drastically.

color. Comparison between Figure 5.2 (both anisotropic energy and mobility) and 5.6 (only energy is anisotropic) and experimental series of Figures 4.19 gives a conclusion that incorporation of anisotropic mobility along with anisotropic energy benefits in better agreement with the experimental results for the region consisting of green grains.

## 5.2 Quantitative comparison between the normal and abnormal grain growth models

In the Introduction Chapter it was shown that normal grain growth (NGG) does not predict experimental results. Therefore, anisotropic model was tested during this thesis work. But it is important to compare both the isotropic and anisotropic models to see

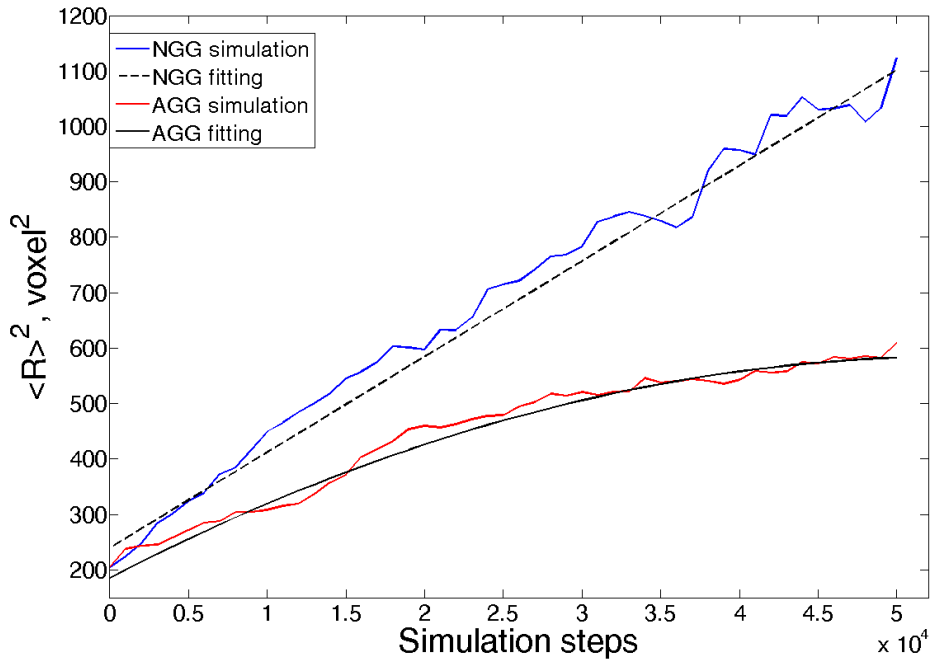


FIGURE 5.7: Square of the average grain radius as a function of simulation steps. Normal grain growth clearly follows linear behavior, while anisotropic model is best fitted with second-order polynomial, proving that the abnormal grain growth is observed.

if the anisotropic model gives closer match with the experiment or not. By anisotropic model further on would be considered the model with both anisotropic energy and mobility and cutoff misorientation  $\theta_m = 32^\circ$  as having so far qualitatively the closest match with experiment.

First thing that should be discussed, if the anisotropic model really provokes the abnormal grain growth during the simulation or not. According to the equation

$$\langle R \rangle^2 = \langle R_0 \rangle^2 + kt, \quad (5.1)$$

where  $\langle R_0 \rangle$  is the initial mean radius of the grains,  $\langle R \rangle$  is the mean radius at time  $t$  and  $k$  is a growth rate. Figure 5.7 illustrates these curves and fittings.

It can be noticed that NGG data can be fitted very well with linear function, while the data for abnormal growth is fitted nicely with second-order polynomial function, which concludes that the data for the AGG is non-linear and therefore, deviates from normal growth. From the experimental results seen before, abnormal grain growth phenomenon definitely exists during the annealing process, therefore plotted square of the average grain radius as a function of annealing time also shows deviation from the linear behavior (Figure 5.8). Experimental and simulation results cannot be directly compared, because

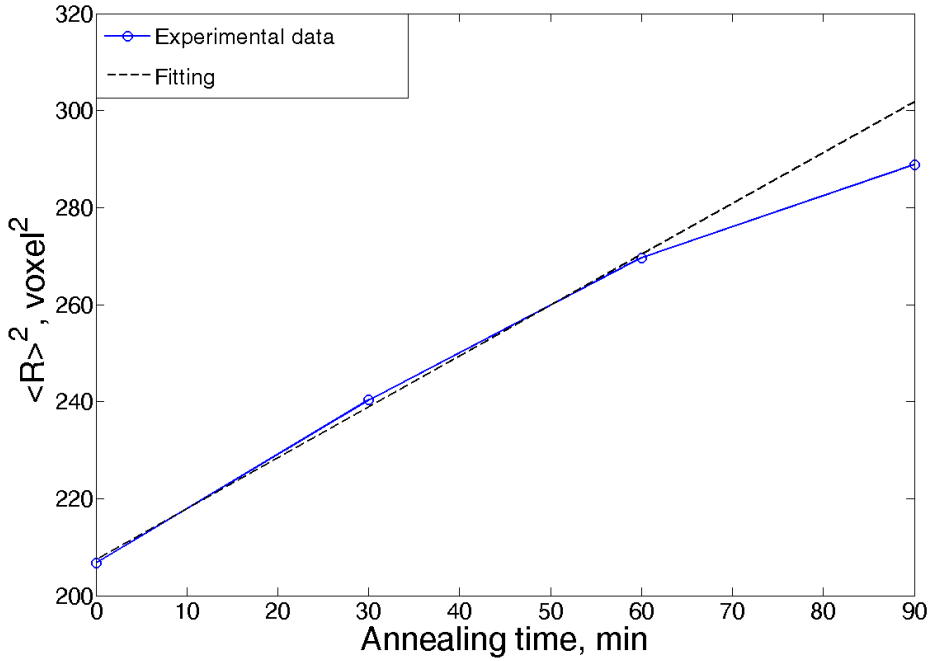


FIGURE 5.8: Square of the average grain radius in experiment as a function of annealing time. Deviation from the linear behavior comes from the abnormal grain growth phenomenon.

the proper time scale is needed for the simulation to relate with experiment. For both the NGG and AGG simulations was not possible to find the consistent scaling with experiment.

Second thing was to investigate that if the morphology in the anisotropic case is closer to experimental values than for isotropic one. Starting with the same microstructure, experimental time steps 30 min, 60 min and 90 min was important to compare with NGG and AGG simulation results. Model for the calculation of the correlation coefficient between the experimental and simulation results is a simple pixel by pixel comparison. All the voxels in the sample were initially labeled with unique grain index, so that could be distinguished between each other. Thus, the correlation coefficient is calculated by the following equation:

$$c = \frac{N_{same}}{N_{total}} = 1 - \frac{N_{diff}}{N_{total}} \quad (5.2)$$

where  $N_{total}$  is the total amount of pixels,  $N_{same}$  is the amount of pixels having same grain label and  $N_{diff}$  is the amount of pixels that are different in terms of grain index.

The microstructure was divided into two regions, as shown in Figure 5.9. The one to the left was called “abnormal grain” region, and the one to the right was called “matrix”

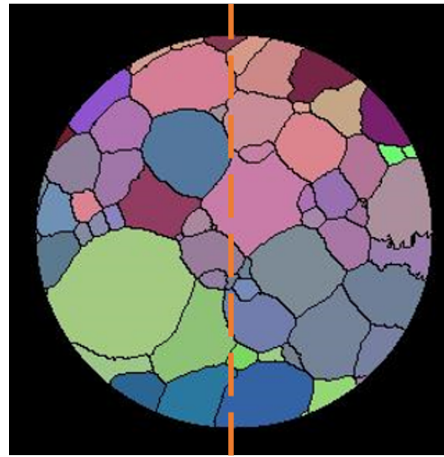


FIGURE 5.9: Division of the microstructure into two regions. Left from the dashed line is “abnormal grain” region and the one to the right is “matrix” region.

region. Intention of such division comes from the fact, that simulation results shown in Figure 5.2, show that the green grain is becoming bigger with the same rate as the matrix grains, while, as can be seen from Figure 4.19, in experiment the matrix moves much slower comparing to the abnormal green grain. That’s why comparison of the whole simulation microstructure with experimental one would not be consistent. Therefore, it was decided to separate the low-angle grain boundary matrix region from the abnormal grain and its neighbors, and compare those regions individually with the experimental results. Resulting curves for the correlation coefficient as a function of simulation steps for both normal and abnormal simulation are shown in Figure 5.10 and the peak values together with confidence intervals are summarized in Tables 5.1, 5.2, 5.3, 5.4.

Time step	NGG		
	Peak value, simulation step	Peak value, correlation coefficient	Confidence interval width
30 min	2500	0.8	3200
60 min	5000	0.66	3800
90 min	5000	0.67	3700

TABLE 5.1: Normal grain growth correlation data for ”matrix” region.

Time step	AGG		
	Peak value, simulation step	Peak value, correlation coefficient	Confidence interval width
30 min	4000	0.81	6200
60 min	10000	0.68	8000
90 min	16000	0.7	3700

TABLE 5.2: Abnormal grain growth correlation data for ”matrix” region.

Because the peaks of those curves are broad, it was decided to take the range of simulation steps that are close to the peak value. So-called confidence interval is a set of

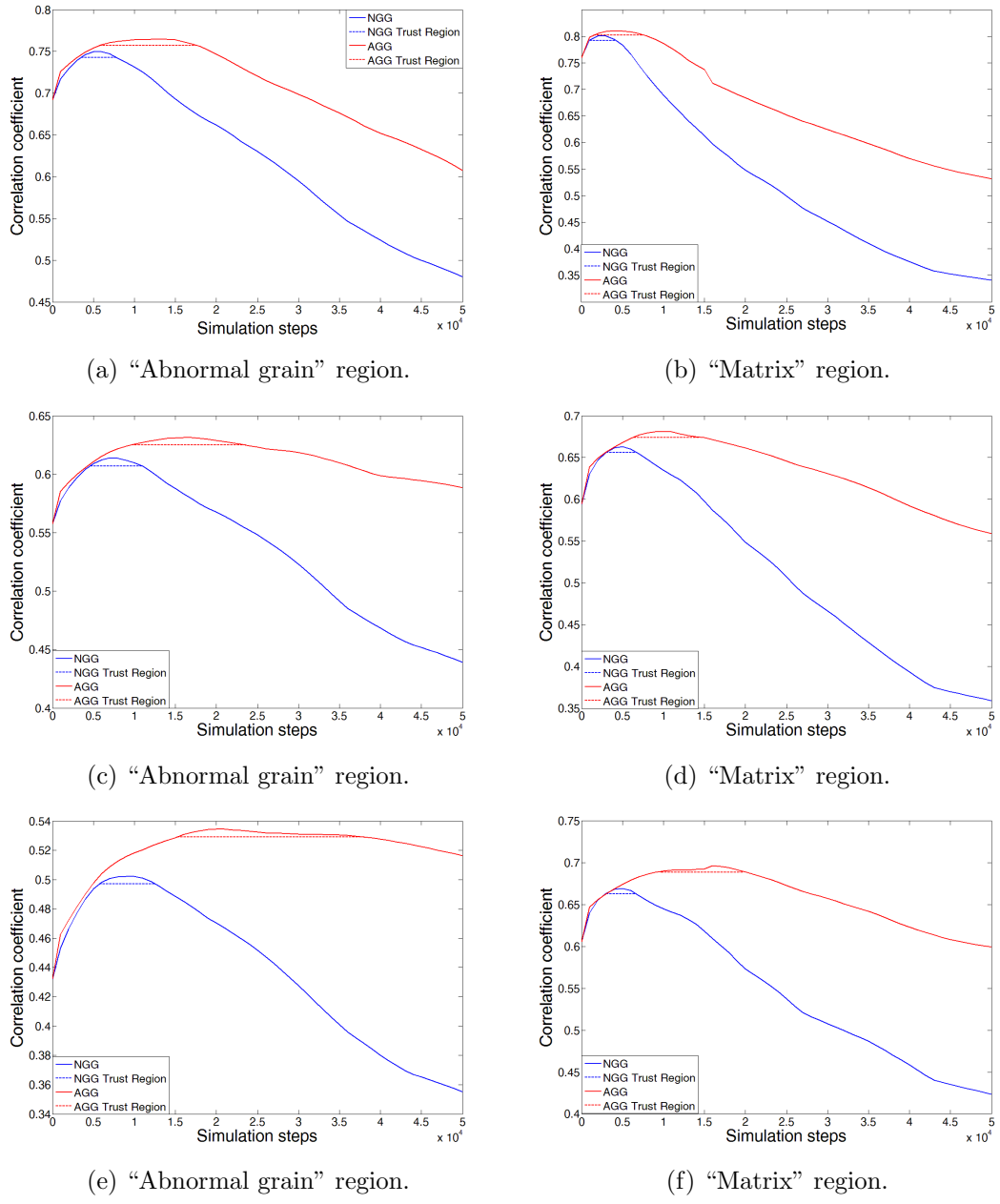


FIGURE 5.10: Correlation coefficient as a function of simulation steps. Plots (a) and (b) is correlation between the simulation and the experimental result at 30 min. Plots (c) and (d) is correlation between the simulation and the experimental result at 60 min. Plots (e) and (f) is correlation between the simulation and the experimental result at 90 min. Anisotropic model shows relatively better matching with experiment than the normal grain growth, because the correlation peak values are bigger than those for isotropic model.

Time step	NGG		
	Peak value, simulation step	Peak value, correlation coefficient	Confidence interval width
30 min	5500	0.75	4300
60 min	7000	0.61	6300
90 min	9000	0.5	6800

TABLE 5.3: Normal grain growth correlation data for "abnormal grain" region.

Time step	AGG		
	Peak value, simulation step	Peak value, correlation coefficient	Confidence interval width
30 min	13000	0.76	12100
60 min	16000	0.63	14000
90 min	16000	0.53	23000

TABLE 5.4: Abnormal grain growth correlation data for "abnormal grain" region.

simulation steps that satisfy the condition of correlation coefficient to be 99% of the maximum value.

Analyzing results shown in Figure 5.10, it can be noticed that, the absolute peak value of the correlation coefficient for anisotropic simulation has higher values than for isotropic simulation. Therefore, it can be concluded that anisotropic model matches better with the experimental results than the isotropic one. Although, the uncertainty is bigger for the anisotropic model, which can be explained by slower average growth rate, as most of the grain boundaries are low-angle grain boundaries and have lower evolution velocity.

Figure 5.11 shows how the peak values for "abnormal grain" and "matrix" region are changing for AGG simulation. Even taking into consideration the confidence interval, it can be noticed that peak values for "abnormal grain region" are higher than for "matrix" region. It can be concluded that in order to come with better agreement with the experimental results somehow either the "matrix" region should be slowed down or "abnormal grain" region accelerated.

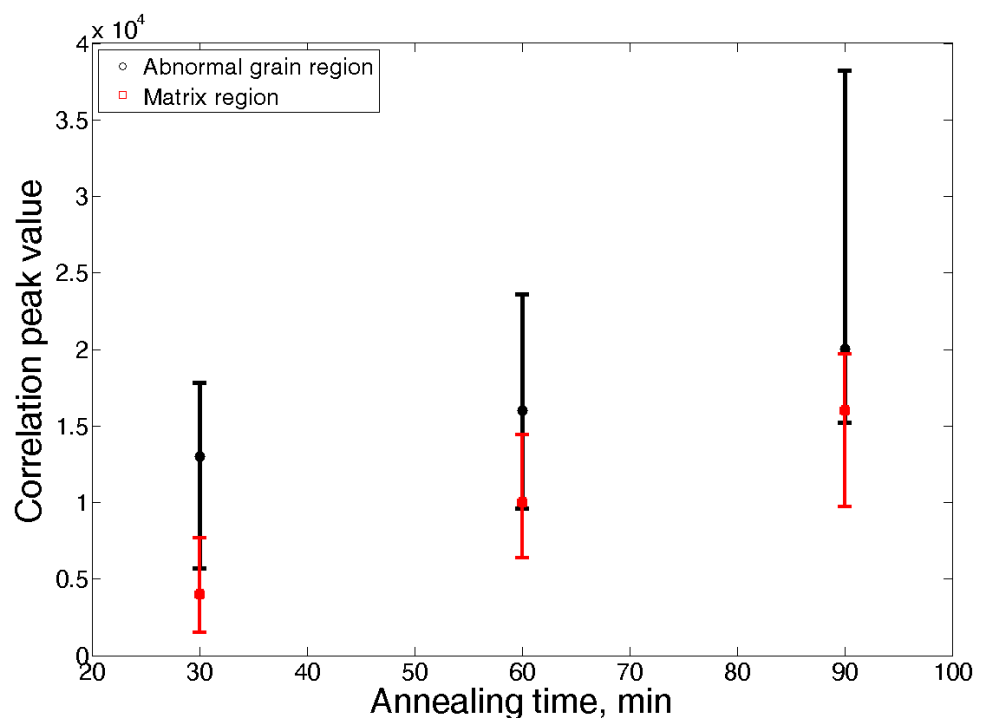


FIGURE 5.11: Correlation peak value dependence on the experimental annealing time for AGG case and different regions. “Matrix” region shows to be faster than “abnormal grain” region. Error bars demonstrate the confidence intervals. To be consistent with experiment “matrix” region should be slowed down.



## Chapter 6

# Summary and Outlook

Prediction of the grain growth in Al-1 wt.% Mg sample with the normal grain growth (NGG) simulation was not successful. Some of the grains that become extremely large in experiment, in the simulation don't come even closer to those sizes. Therefore, this thesis work was intended to investigate if the abnormal grain growth (AGG) model can make simulation results looking closer to experiment than NGG. As was studied before, the investigated material has a strong texture, which implies that the grain boundary energy and mobility should depend on the misorientation between adjacent grains. Anisotropy in the grain boundaries allows some certain grains to get the growth rate domination over slowed down matrix.

Conventional phase-field method cannot handle the anisotropic model of the grain boundaries. Therefore, special algorithm derived by Moelans *et al.* was adopted to cope with different anisotropic models, trying to bring closest match with experimental results. In order to get fast response on how different phenomenological parameters affect the resulting microstructure, 2D simulations were first performed instead of time consuming 3D ones. But investigation of different cutoff misorientations in two-dimensional scale didn't show significant differences between the resulting microstructures. Assuming that topology plays a big role in the grains evolution process, only 3D simulation was performed for further studies. As long as investigation of the whole 3D microstructure is a complicated process, concentration was paid only to a certain slice, where abnormal grain growth was observed in the experiment.

Different anisotropic models were investigated, namely, anisotropic energy with constant mobility, constant energy with anisotropic mobility and cooperation of anisotropic energy together with anisotropic mobility. Each of these models were studied for different values of cutoff misorientations. Values below  $15^\circ$  were essentially chosen because vast majority of the grain boundaries have misorientations ranging from  $0^\circ$  to  $20^\circ$ . Results

have shown that out of all these simulation approaches the best possible match with experiment could be achieved by using anisotropic energy along with anisotropic mobility and cutoff misorientation equal to  $15^\circ$ . But the actual morphology of this simulation was still different than the one in the experiment. In order to improve the existing match different approaches were tried.

Distribution of the misorientations in the two-dimensional experimental slice gave the cue to shift the cutoff misorientation to higher values, namely  $\theta_m = 32^\circ$ . Simulation with this cutoff misorientation and both anisotropic energy and mobility allowed the desired grain to grow bigger in size. But the matrix grains were growing at the same rate as this grain, which contradicts with the experimental results. Following attempts to increase the value of energy plateau resulted in even worse microstructures. Explanation for that is the strong effect of the grains topology, how sizes of different grains affect the evolution. From this qualitative analysis was concluded that for the region of the desired grain, the best match with experiment could be achieved by the model, which involves anisotropic energy along with anisotropic mobility, value of energy plateau  $0.25J/m^2$  and cutoff misorientation  $\theta_m = 32^\circ$ . It was essential to prove that anisotropic model has benefit over the isotropic one. Method for correlation investigation between the simulation results and experimental ones was derived, based on a simple pixel by pixel comparison, however, giving realistic estimations. Plot of correlation coefficient as a function of simulation step for different annealing times proved that anisotropic model gives closer matching with experiment than the isotropic one due to higher values of the curves peaks. Trust regions of the anisotropic model are noticeably wider than those of the isotropic one, which is simply explained by the fact that in isotropic model all grain boundaries have high velocity and in the anisotropic it is slowed down. Therefore, for the same amount of simulation steps anisotropic microstructure changes relatively slower than isotropic one.

In this thesis work Read-Shockley shape for anisotropic behavior was used. In future it is possible to investigate different shapes of the misorientation dependence in order to solve the problem of the matrix grains having same growth rate as the abnormal grain.

# Bibliography

- [1] W. D. Callister and D. G. Rethwisch. Materials Science and Engineering: An Introduction. 2009.
- [2] F.J. Humphreys and M. Hatherly. *Recrystallization and Related Annealing Phenomena*. Elsevier, second edition, 2004.
- [3] W. T. Read and W. Shockley. Dislocation models of crystal grain boundaries. *Phys. Rev.*, 78(3):275–289, 1950.
- [4] A. Lasalmonie and J. L. Strudel. Influence of grain size on the mechanical behaviour of some high strength materials. *J. Mater. Sci.*, 21:1837–1852, 1986.
- [5] J.E. Burke and D. Turnbull. Recrystallization and grain growth. *Prog. Met. Phys.*, 3:220–292, January 1952.
- [6] M. Hillert. On theories of growth during discontinuous precipitation. *Metall. Trans.*, 3(11):2729–2741, 1972.
- [7] S. Yip. *Handbook of Materials Modeling. Volume I: Methods and Models*. Springer, 2005.
- [8] Wikipedia. Grain growth — Wikipedia, The Free Encyclopedia, 2015.
- [9] N.P. Goss. New Development in Electrical Strip Steels Characterized by Fine Grain Structure Approaching the Properties of a Single Crystal. *Trans. Am. Soc. Met.*, 23:511–531, 1935.
- [10] M. Shirdel, H. Mirzadeh, and M.H. Parsa. Abnormal grain growth in AISI 304L stainless steel. *Mater. Charact.*, 97:11–17, November 2014.
- [11] C. Zener and Smith. C. Grains, Phases and Interfaces: Interpretation of Microstructures. *Trans. Metall. Soc. AIME*, 175:15–51, 1948.
- [12] A. D. Rollett, D. J. Srolovitz, and M. P. Anderson. Simulation and Theory of Abnormal Grain Growth - Anisotropic Grain Boundary Energies and Mobilities. *Acta Metall.*, 37(4):1227–1240, 1989.

- [13] O. Engler and V. Randle. *Introduction to texture analysis: macrotexture, microtexture, and orientation mapping*. 2010.
- [14] H.R. Wenk U.F. Kocks, C.N. Tomé and H. Mecking. *Texture and Anisotropy: Preferred Orientations in Polycrystals and their effects on Materials Properties*. Cambridge University Press, 2000.
- [15] H. Beck, P.A. and Hu. *Trans. Met. Soc. A.I.M.E.*, 194:83, 1952.
- [16] W. Bowles, J.S. and Boas. *J. Inst. Met.*, 74:501, 1948.
- [17] J.L. Burgers, W.G. and Snoek. *Z. Met.*, 27:158, 1935.
- [18] E. A. Holm, G. N. Hassold, and M. A. Miodownik. On misorientation distribution evolution during anisotropic grain growth. *Acta Mater.*, 49:2981–2991, 2001.
- [19] Wikipedia. Euler angles — Wikipedia, The Free Encyclopedia, 2015.
- [20] J. K. Mackenzie. Second Paper on Statistics Associated with the Random Disorientation of Cubes. *Biometrika*, 45(1/2):229–240, 1958.
- [21] K. Szwietrzka, J. Pospiech, and F. Haessner. Reduction of Misorientations Between Two Cubic Crystals Into the Base Domain of Axis–Angle Space. *Textures Microstruct.*, 12(4):233–242, 1990.
- [22] K. Mehnert and P. Klimanek. Monte Carlo simulation of grain growth in textured metals. *Scr. Mater.*, 35(6):699–704, September 1996.
- [23] Y. Enomoto and R. Kato. Scaling behavior of two-dimensional vertex model for normal grain growth. *Acta Metall. Mater.*, 38(5):765–769, May 1990.
- [24] Y. Liu, T. Baudin, and R. Penelle. Simulation of normal grain growth by cellular automata. *Scr. Mater.*, 34(11):1679–1683, June 1996.
- [25] Michael Tonks, Paul Millett, Wei Cai, and Dieter Wolf. Analysis of the elastic strain energy driving force for grain boundary migration using phase field simulation. *Scr. Mater.*, 63(11):1049–1052, November 2010.
- [26] J. W. Cahn and J. E. Hilliard. Free Energy of a Nonuniform System. I. Interfacial Free Energy. *J. Chem. Phys.*, 28(2):258–267, 1958.
- [27] Samuel M. Allen and John W. Cahn. A microscopic theory for antiphase boundary motion and its application to antiphase domain coarsening. *Acta Metall.*, 27(6):1085–1095, 1979.

- [28] Long Qing Chen and Wei Yang. Computer simulation of the domain dynamics of a quenched system with a large number of nonconserved order parameters: The grain-growth kinetics. *Phys. Rev. B*, 50(21):15752–15756, 1994.
- [29] I. Steinbach, F. Pezzolla, B. Nestler, M. Seeßelberg, R. Prieler, G.J. Schmitz, and J.L.L. Rezende. A phase field concept for multiphase systems. *Phys. D Nonlinear Phenom.*, 94(3):135–147, July 1996.
- [30] Nele Moelans, Bart Blanpain, and Patrick Wollants. An introduction to phase-field modeling of microstructure evolution. *Calphad Comput. Coupling Phase Diagrams Thermochem.*, 32(2):268–294, 2008.
- [31] M.P. Anderson, D.J. Srolovitz, G.S. Grest, and P.S. Sahni. Computer simulation of grain growth—I. Kinetics. *Acta Metall.*, 32(5):783–791, May 1984.
- [32] D. Fan and L.-Q. Chen. Computer simulation of grain growth using a continuum field model. *Acta Mater.*, 45(2):611–622, 1997.
- [33] C.E. Krill III and L.-Q. Chen. Computer simulation of 3-D grain growth using a phase-field model. *Acta Mater.*, 50(12):3059–3075, July 2002.
- [34] D. Rodney, Y. Le Bouar, and A. Finel. Phase field methods and dislocations. *Acta Mater.*, 51(1):17–30, January 2003.
- [35] Christian Miehe, Martina Hofacker, and Fabian Welschinger. A phase field model for rate-independent crack propagation: Robust algorithmic implementation based on operator splits. *Comput. Methods Appl. Mech. Eng.*, 199(45-48):2765–2778, November 2010.
- [36] M.S. Park, S.L. Gibbons, and R. Arróyave. Phase-field simulations of intermetallic compound evolution in Cu/Sn solder joints under electromigration. *Acta Mater.*, 61(19):7142–7154, November 2013.
- [37] N. Moelans, B. Blanpain, and P. Wollants. Quantitative analysis of grain boundary properties in a generalized phase field model for grain growth in anisotropic systems. *Phys. Rev. B - Condens. Matter Mater. Phys.*, 78(2), 2008.
- [38] T. Young. An Essay on the Cohesion of Fluids. *Phil. Trans. R. Soc. Lond.*, 95: 65–87, 1805.
- [39] U. Czubayko, V.G. Sursaeva, G. Gottstein, and L.S. Shvindlerman. Influence of triple junctions on grain boundary motion. *Acta Mater.*, 46(16):5863–5871, 1998.
- [40] N. Moelans, B. Blanpain, and P. Wollants. Quantitative phase-field approach for simulating grain growth in anisotropic systems with arbitrary inclination and misorientation dependence. *Phys. Rev. Lett.*, 101(2):1–4, 2008.

- [41] A. Kazaryan, Y. Wang, S.A. Dregia, and B.R. Patton. Grain growth in anisotropic systems: comparison of effects of energy and mobility. *Acta Mater.*, 50:2491–2502, 2002.
- [42] J. Gruber, H. M. Miller, T. D. Hoffmann, G. S. Rohrer, and A. D. Rollett. Misorientation texture development during grain growth. Part I: Simulation and experiment. *Acta Mater.*, 57(20):6102–6112, 2009.

## *Acknowledgements*

First of all, I want to express my gratitude to Prof. Dr. Carl Krill, who was giving during all my thesis work very helpful insights and suggestions. I appreciate very much that he was allocating his time to provide professional and nice discussions. I also thank Prof. Dr. Peter Unger for being my second examiner.

Also my very great respect goes to M.Sc. Mingyan Wang, who was supervising me during this thesis work. His high professional skills and kindness made it possible to have immediate discussions whenever I had any question or problem. I am also thankful for his important corrections for this thesis.

One more person whom I should be thankful for is M.Sc. Jules Dake. I appreciate his time spent on helping me with this thesis and giving motivation to be more optimistic about my results.